

Ing. Ondrej Szabó

Author's report on the dissertation thesis

SPUTTERED ZNO THIN FILMS AND AU NANOSTRUCTURES

for the acquisition of: academic title philosophiae doctor, PhD.
in study programme: Electronics and Photonics
and study field: 5.2.13 Electronics

Date and place: In Bratislava, January 2019

**SLOVAK UNIVERSITY OF TECHNOLOGY IN BRATISLAVA
FACULTY OF ELECTRICAL ENGINEERING AND INFORMATION TECHNOLOGY**

Ing. Ondrej Szabó

Author's report on the dissertation thesis

SPUTTERED ZNO THIN FILMS AND AU NANOSTRUCTURES

for the acquisition of: academic title philosophiae doctor, PhD.

in study programme: Electronics and Photonics

and study field: 5.2.13 Electronics

Date and place: In Bratislava, January 2019

The dissertation thesis was prepared in full time attendance form

at the Institute of Electronics and Photonics, Slovak University of Technology
in Bratislava, Faculty of Electrical Engineering and Information Technology

Submitter: **Ing. Ondrej Szabó**
Institute of Electronics and Photonics, Slovak University of Technology
in Bratislava, Faculty of Electrical Engineering and Information Technology
Ilkovičova 3, 812 19 Bratislava, Slovak republic

Supervisor: **prof. RNDr. Vladimír Tvarožek, CSc.**
Institute of Electronics and Photonics, Slovak University of Technology
in Bratislava, Faculty of Electrical Engineering and Information Technology
Ilkovičova 3, 812 19 Bratislava, Slovak republic

Consultant: **Ing. Soňa Kováčová, PhD.**
Institute of Electronics and Photonics, Slovak University of Technology
in Bratislava, Faculty of Electrical Engineering and Information Technology
Ilkovičova 3, 812 19 Bratislava, Slovak republic

Opponents: **doc. Ing. Jozef Novák, DrSc.**
Institute of Electrical Engineering, Slovak Academy of Sciences
Dúbravská cesta 9, 841 04 Bratislava, Slovak republic

prof. Ing. Dušan Pudiš, PhD.
Department of Physics, Faculty of Electrical Engineering, University of Žilina
Univerzitná 12, 010 26 Žilina, Slovak republic

Author's report sent on:

Date of dissertation thesis defence:

at Slovak University of Technology in Bratislava, Faculty of Electrical Engineering
and Information Technology, Ilkovičova 3, 812 19
Bratislava, Slovak republic

prof. Dr. Ing. Miloš Oravec
Dean

Contents

1	Prologue and proposition of the thesis.....	3
2	Introduction.....	4
2.1	Nanostructured ZnO thin films.....	4
2.2	Plasmonic metal nanoparticles for sensor applications	5
3	Experimental methods	6
3.1	Preparation of nanostructured ZnO thin films with gold nanostructures	6
4	Results and discussion	8
4.1	Nanocolumnar ZnO:Al thin films.....	8
4.2	Nanoisland arrays (NIA) Au nanostructures	13
4.3	Universal size-scaling model for shift plasmon resonance	22
4.4	Potential applications of Au NIA in bio-chemical optical sensorics.....	25
5	Conclusion	30
6	Resumé.....	31
7	References.....	34

1 Prologue and proposition of the thesis

A thin film can be characterised as a "two-dimensional" structure because the thickness of the third dimension is so small (from 1 μm to 1 nm) that the surface-to-volume ratio is relatively large (up to 10^6). A decrease in the distance between two surfaces and their interaction has a decisive influence on the internal physical and chemical properties of thin layers, and leads to the emergence of completely new phenomena. Changes in the chemical composition also make the properties of thin layers very diverse, and these may differ significantly from the bulk material. In general, thin films create a "bridge" between macro- and nano-systems, and the development and production of modern microsensors cannot be achieved without the use of thin film technologies.

This study focuses on a combination of ZnO thin films and gold nanostructures. ZnO doped with Al (ZnO:Al) or Ga (ZnO:Ga) belongs to the group of transparent conductive oxide (TCO) thin films; these have specific electronic and optical properties that are applicable in solar cells, optoelectronics and sensorics. Of the nanostructured noble metals, gold is of particular importance due to its stability and its unique electrochemical and optical properties. The morphology of the surface of gold is the feature that most strongly influences its functional properties. Gold nanostructures are often prepared by electrochemical deposition methods [1], but there are a few reports on sputtered micro- and nano-structures [2–4]. Research into Au nanostructures sputtered onto both glass and columnar TCO thin films is important because the results are applicable for biochemical sensors [5].

The purpose of this study is to develop, study and optimise a technology that results in the formation of Au nanostructures on TCO ZnO:Al (ZnO:Ga) thin films or Corning glass substrates. This thesis is therefore divided into several chapters, which focus on the following areas:

- (i) A study of the sputtering of nanocolumnar ZnO:Al thin films and their complex characterisation (i.e. their surface morphology, crystalline structure, electrical and optical characterisation);
- (ii) A study of the influence of radiofrequency (RF) diode sputtering power on the morphology of ultrathin gold layers deposited on ZnO:Al (ZnO:Ga) thin film or glass substrates;
- (iii) A study of the surface plasmon absorption of Au nanostructures formed on glass or ZnO:Al (ZnO:Ga) substrates; and
- (iv) A study of the surface-enhanced Raman spectroscopy (SERS) response of Au nanostructures formed on ZnO:Al substrates functionalised with 11-mercaptopundecanoic acid (11-MUA) [5,6].

This work is expected to contribute to the development of simple and efficient sputtering and thermal annealing technologies for the preparation of transparent conductive oxide ZnO:Al or ZnO:Ga thin films with nanocolumnar structures and gold plasmonic nanoparticles and nanostructures with minimised photolithographic processing. This study will expand the existing knowledge of the physico-chemical properties of the nanostructured interfaces between doped ZnO layers and Au nanostructures via a complex study using comparative characterisation techniques.

2 Introduction

2.1 Nanostructured ZnO thin films

Zinc oxide (ZnO) is an n-type semiconductor with a wide band gap (3.3 eV at 300 K) that is used as a promising candidate to replace other wide band gap semiconductors, such as indium tin oxide (ITO) [7], which is primarily used as a transparent electrode in optoelectronic devices. The hexagonal structure of wurtzite is the most common crystalline phase of ZnO (**Figure 2.1**).

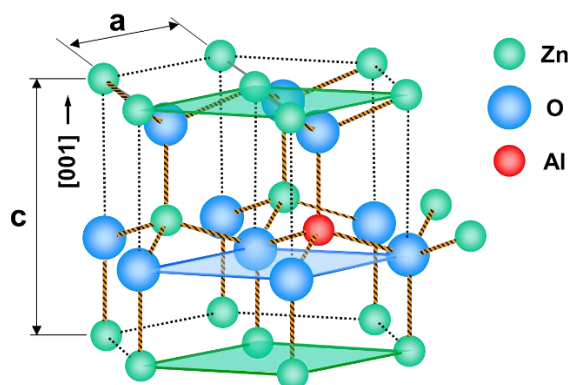


Figure 2.1 Schematic representation of the wurtzite ZnO structure doped with Al (AZO)

It has been found that the conductivity of ZnO films increases when doped with aluminium or gallium (so-called AZO or GZO films, respectively). In general, the doping of ZnO with Al causes a rearrangement of the ZnO grid and generates a free electron in the conduction band [5,7,8]. Both AZO and GZO films are TCO films, which have recently attracted attention due to their nontoxic nature, cost-effectiveness and easy fabrication [7]. TCOs based on ZnO are used in thin film solar photovoltaic cells, and ZnO nanostructures (such as clusters, wires, nanotextured surfaces and nanocolumnar crystallinity), have shown a particularly wide range of potential applications for advanced photon management design in the novel generation of solar cells [9].

However, it is worth noting that a sensor based on ZnO:Al still has certain limitations. Some sensor properties (such as sensitivity) can be improved by several techniques, e.g. by nanostructuring of the active surface of a sensor or by combining it with plasmonic structures based on noble metals.

For example, a columnar morphology can be achieved by the nanostructuring of ZnO films, which is used to tailor the desired anisotropic optical properties. These polycrystalline columnar structures are also used for the fabrication of sculptured thin films, a new class of optical materials [8,10,11]. In the case of columnar growth along the c axis, the Zn^+ or O^- surface may have a specific surface termination. (**Figure 2.2**). These terminated polar surfaces can improve the molecular bond, which is advantageous for biochemical imaging.

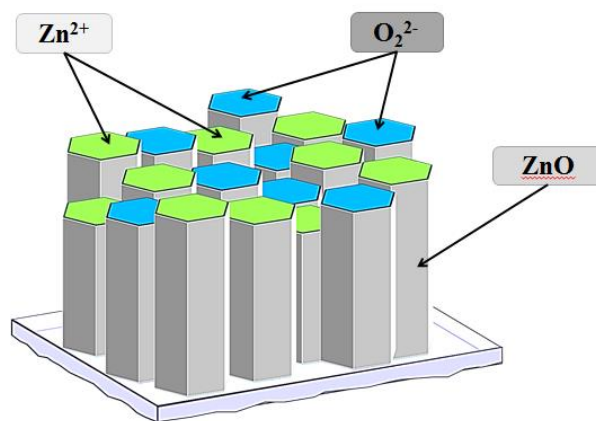


Figure 2.2 Nanocolumnar structure of a ZnO film

Nanostructured ZnO thin films, and particularly nanotextured and nanoporous ZnO thin films, are also employed in gas- and bio-sensors since they exhibit non-toxicity, strong adsorption ability, high catalytic efficiency and electron transfer capability [12–14]. The morphology and crystallographic structure of ZnO thin films (thickness, grain size, texture, faceting, surface geometry, agglomeration and porosity) have a significant influence on the main characteristics of biochemical sensors.

2.2 Plasmonic metal nanoparticles for sensor applications

Noble metal nanostructures have been widely studied in label-free biological sensor applications [15,16] using localised surface plasmon resonance (LSPR), which (as discussed above) is a coherent oscillation of the free electron gas in metal nanoparticles excited by electromagnetic radiation, particularly in the optical range. Trends in the development of plasmonic technologies include efforts to produce Au or Ag nanoparticles of controllable shape, size and porosity, with the aims of improving the LSPR tunability and simplifying the technological procedure [17]. Recently, innovative physical technologies have been developed as an alternative to traditional chemical reduction methods for obtaining metal (Au, Ag) nanoparticles. These technologies include laser ablation or pulsed deposition, electron-beam or nanosphere lithography [18], thermally induced dealloying and dewetting on pre-patterned substrates by nanoimprint lithography [19], electron-beam lithography [20] and evaporation [21], depositions or sputtering of nanostructured or porous Au films and nanoisland arrays [2,22,23]. The application of LSPR sensors requires a solid transparent support, e.g. a glass substrate or TCO films.

In this work, our aim was to simplify the technological procedures of the formation of Au plasmonic nanostructures (e.g. in an island-like shape) directly by sputtering, without the use of any lithographic process. The structural, morphological and optical properties of sputtered Au nanoisland arrays (NIA) (on bare Corning glass, or GZO films sputtered on Corning glass substrates) were studied and compared to the universal size-scaling plasmon coupling model [24,25]. A description of the plasmonic behaviour of sputtered Au NIA is presented using the technological parameters of a thin film, such as the RF power density and the nominal thickness [26].

3 Experimental methods

3.1 Preparation of nanostructured ZnO thin films with gold nanostructures

Continuous and sequential sputtering of ZnO:Al (Ga) films and Au nanoisland arrays using an RF diode system

For the deposition of ZnO:Al thin films, an RF diode sputtering system was used (Perkin/Elmer 2400/8L, installed at the Institute of Electronics and Photonics of FEI STU in Bratislava). Continuous sputtering (**Figure 3.1 a**) of ZnO:Al thin films was performed using the standard static mode of deposition, in which the substrates were placed under the target, with a ceramic target (ZnO+2 wt. % of Al₂O₃, 152.4 mm in diameter) in Ar working gas. Post-deposition annealing of ZnO:Al thin films with a thickness of 560 nm was carried out at 500 °C for 30 min in the forming gas N₂:H₂ (90:10) [27].

Deposition of ZnO:Al (Ga) and Au was performed by sequential mode (dynamic, **Figure 3.1 b**) sputtering [28] using an Au target 203.2 mm in diameter and an Ar atmosphere (pressure 1.3 Pa). The substrates were moved under the target by turning the substrate holder, where the deposition time corresponding to one turn was approx. 9 s. Corning glass substrates (bare or covered by TCO ZnO:Al (Ga) thin film) were heated to 200°C before Au deposition. The influence of RF power on the morphology of Au nanostructures was examined. The sputtering rates were determined from the thicknesses and the time of deposition of homogeneous thin films, which were evaluated using a Dektak profilometer. The amount of sequentially sputtered material was estimated based on the nominal thickness of the film deposited during the period of a single turn (≈ 9 s) under the target. The sputtering rate of Au was dependent on the RF power density, and its values were determined as follows: 0.12 nm/s (for 2.3 mW/mm² RF power density), 0.25 nm/s (4.6 mW/mm²), 0.5 nm/s (9.2 mW/mm²) and 1.0 nm/s (18.5 mW/mm²).

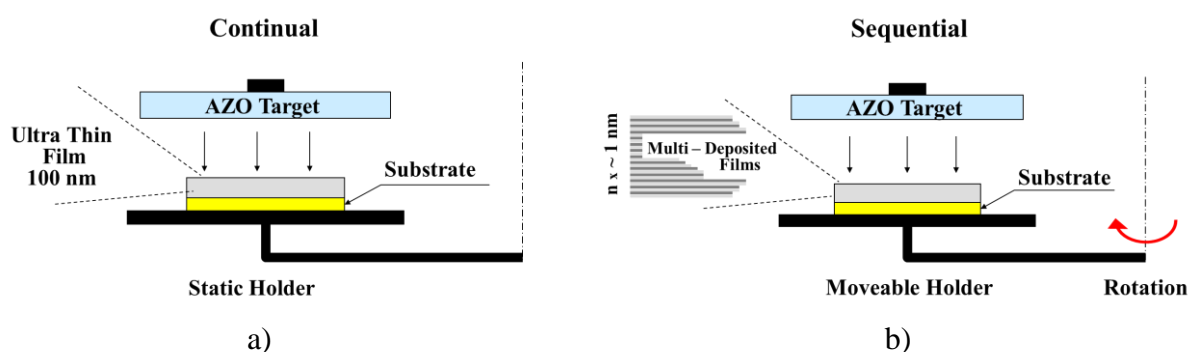


Figure 3.1 Schematic drawing of the a) continual and b) sequential sputtering of ZnO:Al (Ga)

Growth of columnar ZnO thin films

In general, in the field of thin film growth, the early stages are dominant, that is, the formation of nuclei, the growth of clusters and islands and their coalescence. Competing atomistic processes are involved in nucleation and growth [29], i.e. the adsorption, diffusion and binding of particles (involving the surface and interfacial energetics of the substrate and condensing atoms). In the case of columnar thin films, the growth is determined by two main

competing mechanisms: atomic-scale shadowing and surface diffusion [30]. The principle of atomic-scale shadowing (also known as “self-shadowing”) can be described as follows. As the sputtered particle nucleates on the substrate, the region behind the nucleus receives a minimal flux of condensed particles, because this region falls within the “shadow” of the nucleus. Sputtered particles will therefore be deposited only onto the nucleus, thus developing a columnar structure.

Preparation of Au nanoisland arrays

Of the nanostructured noble metals, gold is of particular importance, due to its stability and its unique electrochemical and optical properties. The morphology of gold is the most important parameter affecting its properties. Gold nanostructures are often prepared using electrochemical deposition methods [5].

Our aim was to simplify the technological procedures involved in the formation of Au plasmonic nanostructures (with island-like shape) directly by sputtering, without the use of masking and lithographic processes. We use a single mode of sputtering, i.e. sequential sputtering of Au NIA, on three kinds of substrates:

- (i) Corning glass;
- (ii) Corning glass with sputtered columnar ZnO:Al (or ZnO:Ga) thin films;
- (iii) Corning glass covered by ultrathin Ti film.

Thin gold layers were sputtered on substrates for different sputtering times using RF diode sputtering (Perkin/Elmer 2400/8L), the same technique used for sputtering of ZnO films. The thickness of the sputtered Au layers was within the range 1.5 nm to 126 nm. Sputtering was performed at room temperature inside a vacuum chamber at a basic pressure of about 1.1–2 mbar (1 Pa). A sequential (*dynamic, cyclic*) sputtering method was applied, which has a strong influence on the thickness and homogeneity of the films involved in the sputtering process. Continuous sputtering was used primarily for the deposition of the ZnO film, while sequential sputtering was used for the preparation of gold layers.

In comparison to static sputtering (in which the substrate holder is stable, and the substrates are underneath the target the whole time), cyclic sputtering is a dynamic mode of deposition, in which the substrate holder is not still but rotates continuously underneath the target. The concept of cyclic sputtering is illustrated in **Figure 3.2** [5]. This method allows the deposition of very thin layers. The nominal thicknesses of the Au island films (2–8 nm) that were sputtered from the Au target with a diameter of 203.2 mm at RF power 75–300 W were determined using a Dektak profilometer.

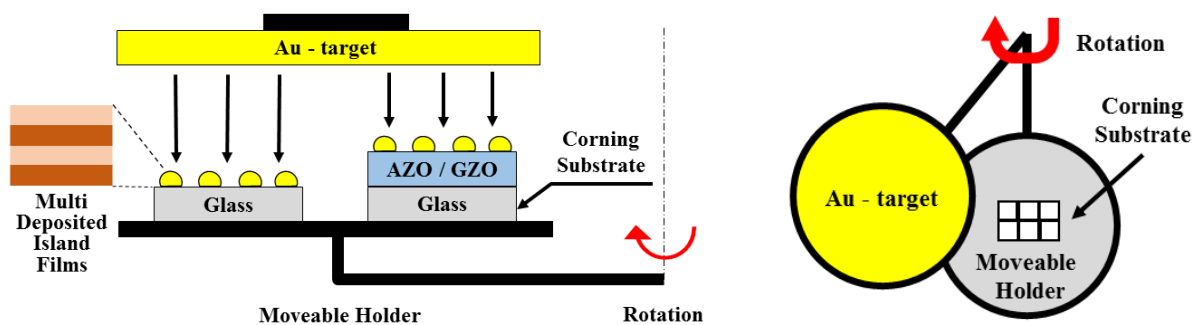


Figure 3.2 Schematic drawing of sequential sputtering of Au NIA

Post-deposition annealing was carried out in the sputtering chamber immediately after deposition in a vacuum at 1 Pa at 300°C for 2 h, and additionally in an external furnace (in air at atmospheric pressure at 500°C for 5 h).

4 Results and discussion

4.1 Nanocolumnar ZnO:Al thin films

Continuous and sequential sputtering of ZnO:Al thin films

a) Morphology of ZnO:Al nanostructure films studied by SEM

An evaluation of the surface morphology using SEM image processing was carried out using ImageJ software (as described in the previous chapter). **Figure 4.1 a** presents the results of SEM image processing for the nanostructured ZnO:Al layers, showing SEM images of the sample surfaces and the corresponding density distribution of the nanostructures. A statistical analysis of SEM images (probability density) showed a log-normal distribution of the upper surface areas of the nanostructures, and their mutual distances were characterised by a Gaussian distribution [5,6,8].

The surface morphology and crystalline structure of sputtered ZnO thin films were influenced by the deposition time, substrate temperature, power density, and the method used (i.e. continuous or sequential sputtering). In comparison with continuous sputtering, the sequential sputtering mode allowed us to achieve very low deposition rates, higher homogeneity and closely controllable 3D coverage [5,6,8].

The structural columnar hierarchy of a continuous sputtered ZnO:Al film is shown in **Figure 4.1 b**. The crystalline structures of the film corresponded to zone 2 of the crystalline structure of our zone representation [5,8,31]. It was observed that continuous sputtering led to the growth of larger columnar grains than in sequential sputtering (a so-called V-shaped growth, **Figure 4.1 c**). This effect was intensified by the self-heating of the growing film during sputtering and by an increase in the deposition time (giving a higher thickness). A similar grain hierarchy was observed in both the experimental results and theoretical simulations [32]. The size of the columnar grains oriented perpendicularly to the substrate was increased in the direction normal to the surface; the upper areas of the grains in the surface plane were characterised by a log-normal distribution of areas A with modulus 1050 nm^2 , and the modulus of the NN grain distances was 65 nm (**Figure 4.1 d**) [8]

b) Electrical properties of ZnO:Al nanostructure films

The electrical properties (resistivity, concentration and mobility of electrons) were estimated using Hall measurements (Ecopia HMS-5300). As is well known, the resistivity of very thin AZO films depends on the AZO “bulk” resistivity, the resistivity caused by electron scattering on columnar grain boundaries, and the resistivity arising from the thickness “size” effect [33]. The surface scattering of electrons must be taken into consideration when thin film thicknesses are $\leq 100 \text{ nm}$, since their average free path is a few tenths of a nanometre in AZO films.

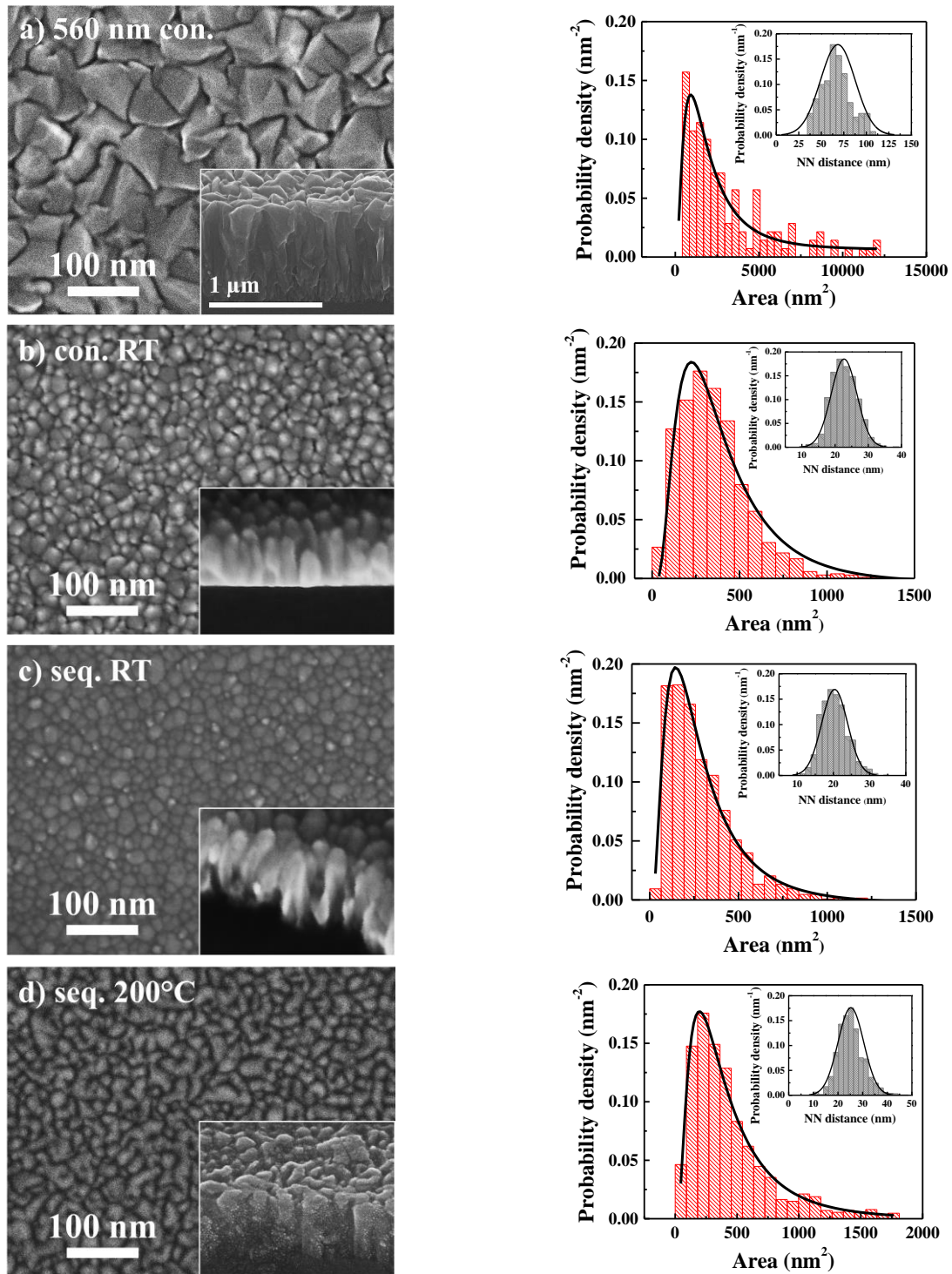


Figure 4.1 Surface morphology of sputtered ZnO:Al layers measured using SEM and the corresponding density distribution of nanostructures. All ZnO:Al films had a final thickness of ~ 100 nm except (a), where the ZnO:Al film was 560 nm thick. Note: The films were prepared either by continuous (labelled as ‘con.’) or sequential (labelled as ‘seq.’) sputtering.

The size resistivity effect is negligible in films with thicknesses of several hundredths of a nanometre where larger crystalline columnar grains are developing. For example, in the case of a sample of thickness 560 nm (**Figure 4.1 a**), the development of larger crystalline columnar grains leads to a decrease in the AZO film resistivity to a value of $1 \times 10^{-2} \Omega \text{ cm}$ and to an increase in the electron mobility of $2.5 \text{ cm}^2/\text{Vs}$ at a concentration of $2 \times 10^{20} \text{ cm}^{-3}$. Assuming electron grain-boundary scattering, the calculated value of the electron mean free path [34] is

30 nm. Ionised impurity scattering becomes dominant in a range of electron concentrations greater than 10^{20} cm^{-3} according to the behaviour of the degenerate semiconductors [34].

When the grain sizes (approx. 10 nm) and the film thickness ($\leq 100 \text{ nm}$) are comparable with the mean free path of electrons, grain boundary and surface scattering of electrons must also be taken into consideration. The calculated values of the electron mean free path in AZO films are usually much smaller than the experimentally observed grain sizes [34] (in our case, these calculated values were approximately 5 nm). Very thin AZO films ($\approx 100 \text{ nm}$ in thickness) exhibit resistivity in the range $0.1\text{--}10 \ \Omega \text{ cm}$ (at electron concentrations of $10^{18}\text{--}10^{19} \text{ cm}^{-3}$) since both grain boundary and surface scattering effects occur (**Figure 4.2**).

Sequential sputtering with the substrate at RT induced the highest resistivity ($\approx 8.6 \ \Omega \text{ cm}$), and the lowest electron mobility ($0.5 \text{ cm}^2/\text{Vs}$) and electron concentration ($\approx 1.5 \times 10^{18} \text{ cm}^{-3}$), for the following reasons: (i) the grain boundaries were increased in size, and thus electron scattering took place; and (ii) numerous Al atoms were located at interstitial positions, where they cannot contribute to the conductivity (**Figure 4.2 a**). The external heating of the substrate to a temperature of 200°C improved both the crystalline structure (**Figure 4.1 d**) and the electrical properties of sequentially sputtered films (by lowering their resistivity ($\approx 0.3 \ \Omega \text{ cm}$) and increasing the electron mobility ($0.8 \text{ cm}^2/\text{Vs}$) and electron concentration ($\approx 2 \times 10^{19} \text{ cm}^{-3}$)).

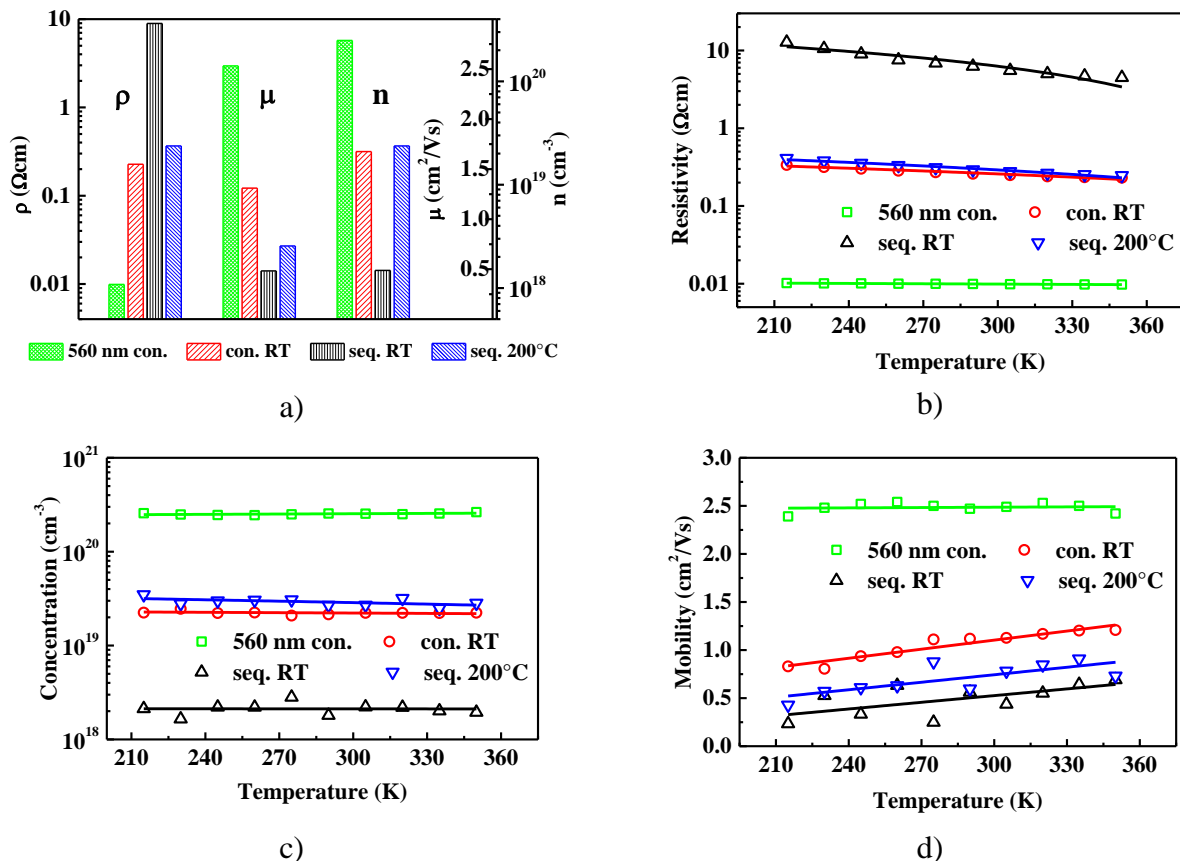


Figure 4.2 Summary of the electrical properties of AZO films with thicknesses of 560 nm (sample labelled as ‘560 nm con.’) and $\approx 100 \text{ nm}$ (samples labelled as ‘con. RT’, ‘seq. RT’ and ‘seq. 200°C ’): (a) electrical properties (resistivity, electron mobility and free electron concentration) at room temperature; (b), (c), (d) temperature dependencies of resistivity, electron concentration and and electron mobility, respectively.

In this case, the surface morphology of the film is characterised by the highest (002) texture with the largest columns (the modulus of the top area was 260 nm^2 , and the size of crystallites was $\langle D_c \rangle = 65 \text{ nm}$).

The electrical properties of the thin films prepared by continuous sputtering at RT and sequential sputtering at 200°C were nearly the same, since self-heating of the substrate occurred during the continuous mode. The decrease in resistivity at temperatures ranging from 200–350 K (**Figure 4.2 b**) is caused by a rise in electron mobility (**Figure 4.2 d**), since the concentration of electrons does not change (all of the impurities are already ionised), as shown in **Figure 4.2 c**. This variation in electron mobility can be explained by a change in the electron scattering as a result of the influence of the gas environment (the ambient air), the temperature at the surface and grain boundary, and the absorption/desorption of water vapour and oxygen in particular (e.g. polar water molecules can condense at temperatures below RT) [5,8].

c) Optical properties of ZnO:Al nanostructure films

The transparency of the continuous and sequentially sputtered AZO films in the Vis range was measured as varying between 80% and 90% (see **Figure 4.3 a**), and the transparencies overlap in the NIR region. The refractive index of the films (~ 2.1 [35]) was close to the value for ZnO (**Figure 4.3 b**).

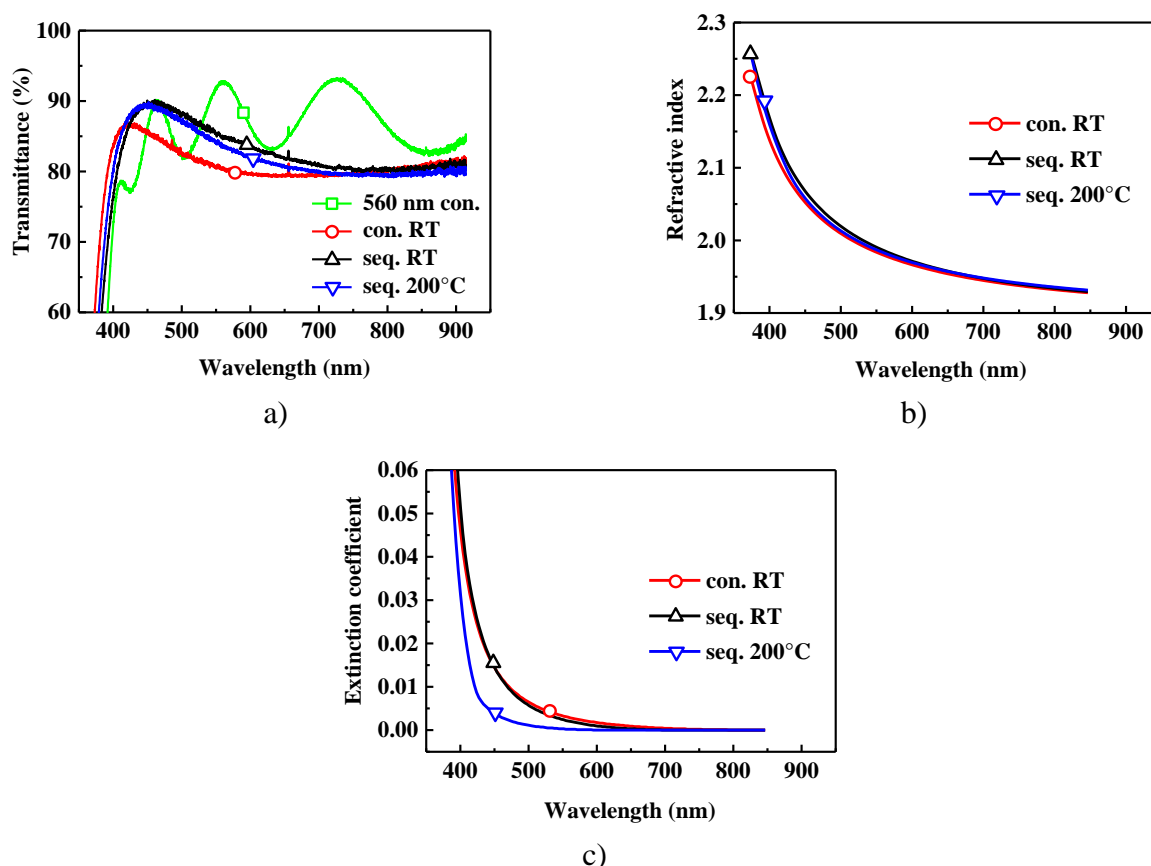


Figure 4.3 Optical properties of various AZO thin films: (a) transmission spectra; (b) refractive index; and (c) extinction coefficient

The imaginary part of the refractive index, known as the extinction coefficient, describes the absorption of the film. Sequentially sputtered films on the substrate heated to a temperature of 200°C exhibited the lowest absorption in the Vis region (**Figure 4.3 c**). The values and spectral dependencies of the refractive index and extinction coefficient are comparable those in

previously published data for sputtered AZO films [8]. The refractive index had values of around 2, and a low extinction coefficient was observed in the range 10^{-2} – 10^{-3} . These optical properties are better than for AZO films obtained using other preparation technologies such as pulsed laser deposition [36] or the sol-gel dip technique [37].

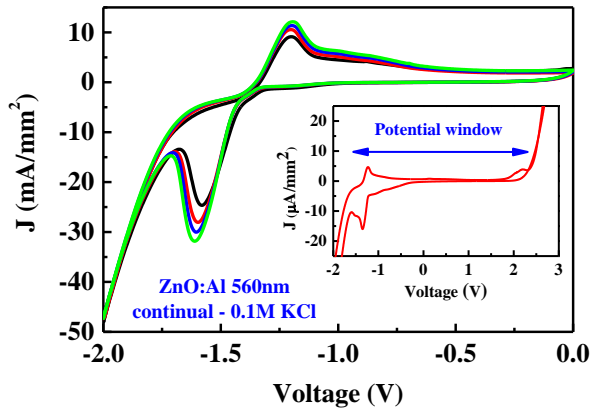
These results are promising for the application of AZO thin films in SERS spectroscopy, since the high refractive index of ZnO promotes the strong confinement of light, thus increasing the SERS effect. In addition, sequential sputtering is a promising technique for preparing plasmonic structures without the use of lithographic processes [8].

Summary of the deposition and properties of ZnO films and proof of concept of electrochemical voltammetric sensor based on a nanocolumnar ZnO:Al film

Our results confirmed the advantages of the use of sputtering to prepare AZO films with a nanocolumnar polycrystalline structure. Here, the significant deposition parameter was the elevated substrate temperature of about 200°C, which primarily influenced the crystalline structure. This sequential sputtering technology was developed for the formation of transparent and very thin conductive AZO films (thicknesses of ≈ 100 nm) which exhibited (in comparison with the continuous sputtering mode): (i) substantial nanocolumnar (002) texture, containing highly ordered crystalline grains (crystallite sizes $\langle D_c \rangle \approx 65$ nm); (ii) low lattice stress gradients ($\approx 10^{-2}$ – 10^{-1} GPa/nm) and microstrains ($\langle \varepsilon \rangle \approx 7 \times 10^{-3}$); (iii) comparable resistivities ($\approx 10^{-1}$ Ω cm); (iv) high optical transparency (≈ 90 %) and an adequate refractive index (≈ 2.0). A particular feature of sequential sputtering was a low deposition rate (on the order of 0.1 nm/s). In addition, the more or less isotropic deposition at working gas pressures of 1 Pa or greater open the way for the use of this sputtering mode in the controllable nanocoating of 3D samples, as proven by the sputtering of a highly consistent coverage (shell) of GaP nanowires [28,38]. The outcomes of the present research allow us to exploit the nanocolumnar structures of ZnO for biochemical sensing applications, as a consequence of their large surface-to-volume ratio and chemically active surface facets [8].

As discussed above, ZnO thin films and nanostructures have several unique advantages (such as high surface area, nontoxicity, good biocompatibility and high electron communication features) for the development of electrochemical biosensors [12,39]. ZnO exhibits a large isoelectric point (ISE ≈ 9.5), meaning that the electrostatic attachment of bio-substances (e.g. proteins) with low ISE ('negatively charged') is straightforward [40]. It is very important to note that ZnO thin films are relatively stable around a neutral pH of 7; this gives ZnO-based sensors much more biocompatibility with biological fluids and species [41], since most biological fluids have a pH of around 7 (e.g. blood has a pH of 7.4 [42]). Hence, in our proof of concept study, we performed an electrochemical experiment in which we used a 0.1 M KCl solution that has properties somewhat similar to those of blood.

In these experiments, the electrochemical behaviour of ZnO:Al was studied using cyclic voltammetry (**Figure 4.4**) with an Ag/AgCl reference electrode at a scan rate of 100 mV/s. These measurements showed two current peaks at -1200 mV and -1600 mV, which correspond to redox reactions on the ZnO:Al electrode [43]. A relative wide potential window (~ 3.5 V) was evaluated, allowing us to detect a wide range of bio-/inorganic species, including heavy metals [5,44].



a)



b)

Figure 4.4 (a) Cyclic voltammogram for ZnO:Al film with thickness 560 nm; (b) photo of the electrochemical cell used in cyclic voltammetry measurements

4.2 Nanoisland arrays (NIA) Au nanostructures

The Au plasmonic nanostructures were directly sputtered on three kind of substrates: Corning glass, Corning glass with sputtered columnar ZnO:Ga or ZnO:Al thin films, and Corning glass covered by ultrathin Ti film. A single mode of sputtering was applied, i.e. the sequential sputtering of an Au NIA for different sputtering times.

SEM analysis revealed that the initial stage of growth of the Au layer is characterised by the formation of isolated islands. In comparison with Au sputtering on ZnO:Ga films, the deposition rate of the Au on the glass substrate is higher, and a continuous coating is formed under the same sputtering conditions. AFM measurements showed that the initial surface roughness of ZnO:Ga is considerably higher (± 10 nm) than the roughness of the glass (± 0.5 nm), and as shown by XRD, the Au layers are polycrystalline with a preferred grain orientation in the (111) direction.

It was also observed that annealing at 300°C for 1 hour leads to a significant change in the morphology of the Au layer, and this influences its electrical and optical properties. Annealing leads to the agglomeration of gold particles and the formation of larger isolated islands. Thin Au layers with thickness $t = 1.5\text{--}126$ nm were formed by RF sputtering on glass substrates at RT inside a vacuum chamber at a basic pressure of about $1 \cdot 10^{-2}$ mbar (1 Pa). The dependence of the grain diameter of Au on the layer thickness shows that the grain growth mechanism predominates by spreading the Au molecules at the grain boundaries. A particle with a diameter of about 5 nm or less has unique catalytic properties.

The structural, morphological and optical properties of sputtered Au NIAs were studied and compared with the results of the universal size-scaling plasmon coupling model [24,25]. A description of the plasmonic behaviour of sputtered Au NIAs is also presented based on thin film technological parameters such as the RF power density and the nominal thickness.

Au NIA sputtered on a glass substrate

A statistical analysis of SEM images of Au surface morphology exhibited a log-normal distribution of the area of the NIA and a Gaussian distribution of the near neighbour distance of

NIA. The centre of the log-normal distribution of the nanoisland areas is labelled as modus A_M and the centre of the Gaussian distribution of the near neighbour distance between nanoislands as modus NN_M .

Sequential sputtering: Varying sputtering power

We used the deposition concept of sequential (cyclic) sputtering [5], as illustrated **Figure 3.2**. In this dynamic mode of deposition, the substrate holder rotated under the target (for a single rotation only).

RF diode sputtering was used for the deposition of Au NIA on Corning glass substrates. The nominal thicknesses of the Au island films (2–8 nm), sputtered from an Au target at an RF power of 75–300 W, were determined using a Dektak profilometer. Post-deposition annealing was carried out in the sputtering chamber immediately after deposition (300°C / 2h).

The specificity of the formation of nanostructures can be highlighted by exploiting the early stages of thin film growth. Sputtered non-continuous island Au films were grown according to the Volmer-Weber model [29], and **Figure 4.5 a** shows the formation of nuclei, clusters and islands and their coalescence. The nominal thickness was measured by the mechanical Talystep method, giving a value that characterises only the “envelope” of the NIA, which implicitly contains data on the amount of deposited material and its distribution, structure and size, including the height of the nanoislands. Their nominal thicknesses were almost linearly proportional to the sputtering RF power (RF power densities), as shown in **Figure 4.5 b**.

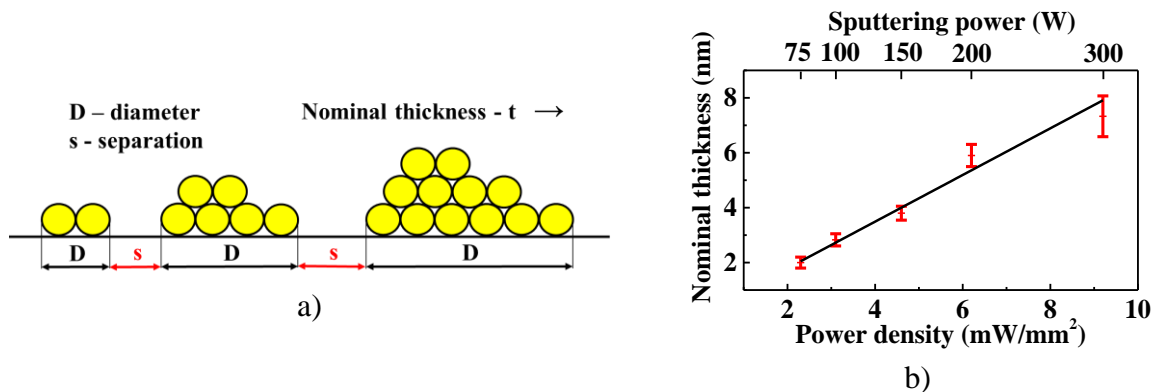


Figure 4.5 a) Schematic model of the early growth stage of sputtered Au island films; b) nominal thickness of Au nanoisland films vs. RF sputtering power (RF power density)

SEM and the open source image processing program ImageJ [45] were used to evaluate the surface morphologies. Statistical analysis of SEM images of the Au surface morphology (**Figure 4.6**) exhibited a log-normal distribution of the area of the NIA and a Gaussian distribution for the near neighbour distance of the NIA.

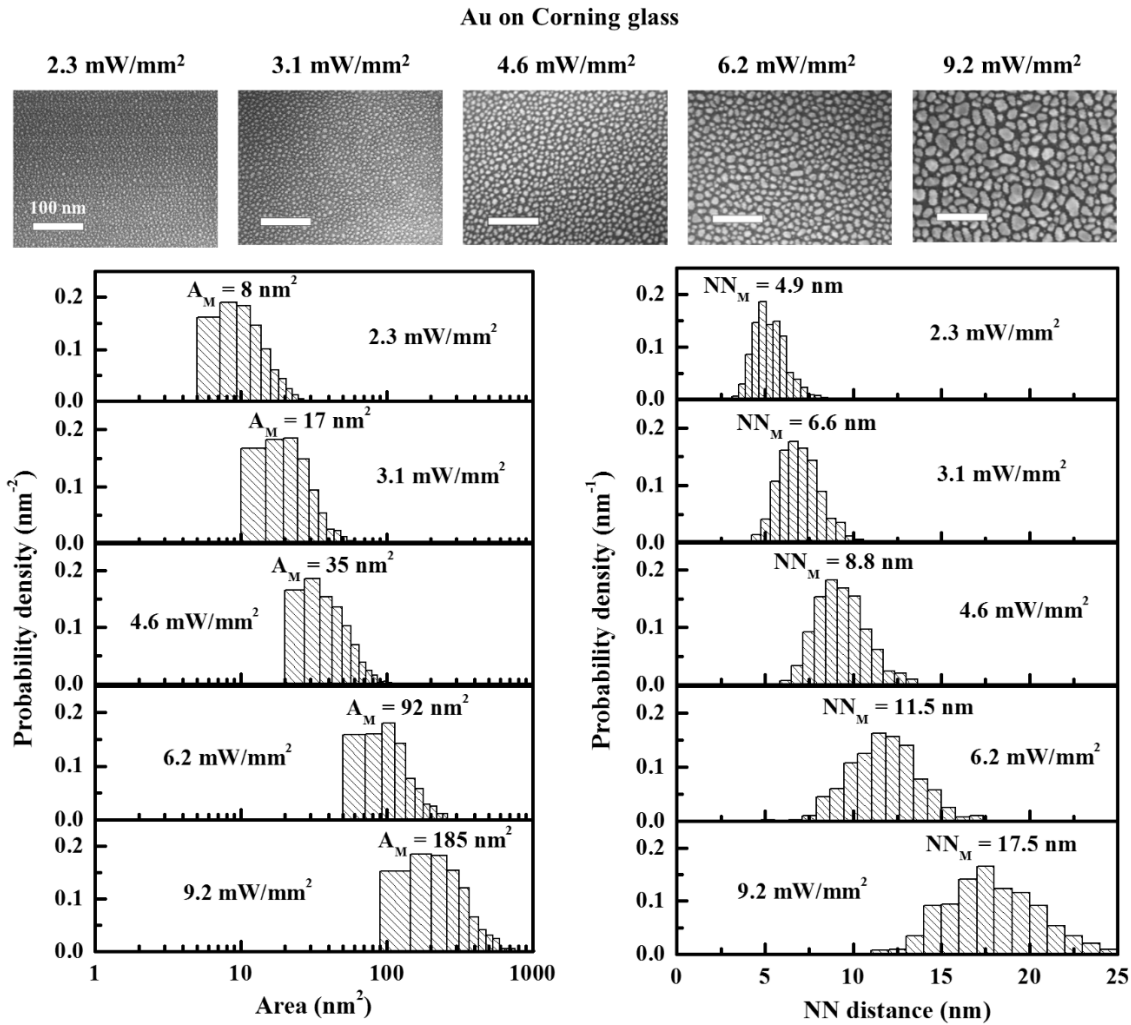


Figure 4.6 SEM images of Au nanoisland arrays sputtered on Corning glass substrate at different power densities / nominal thicknesses: 2.3 mW/mm² / 2.4 nm, 3.1 mW/mm² / 2.8 nm, 4.6 mW/mm² / 3.8 nm, 6.2 mW/mm² / 5.9 nm, 9.2 mW/mm² / 7.3 nm; the statistical distribution of nanoisland areas and near neighbour distance (A_M and NN_M are the corresponding moduses)

An increase in the nominal thickness caused an evident increase of the areas (diameters) of the nanoislands (**Figure 4.6**), although their separations were extended by only a small amount. This varied between 8–185 nm² (Corning glass substrate, **Figure 4.6**) depending on the RF sputtering power density. In both cases, the nanoisland NN distance exhibited a Gaussian distribution.

We used very rough approximations to determine the nanoisland dimension D (assuming a circular shape of the NIA area ($D = 2 \cdot (\sqrt{A_M/\pi})$)) and inter-island separation s from the statistical evaluation SEM images ($s = NN_M - D$). The diameters of the Au NIAs were significantly changed, from 3 nm to 15 nm, while their separation changed slightly from 2 nm to 3 nm with an increase of the sputtering power density.

An XRD analysis indicated that the polycrystalline structure of the Au NIA was preferentially oriented in the [111] direction (**Figure 4.7 a**). The texture of the Au NIA increased with the power density.

The transverse LSPR and the scattering were evaluated using transmission UV-Vis spectroscopy (**Figure 4.7 b**).

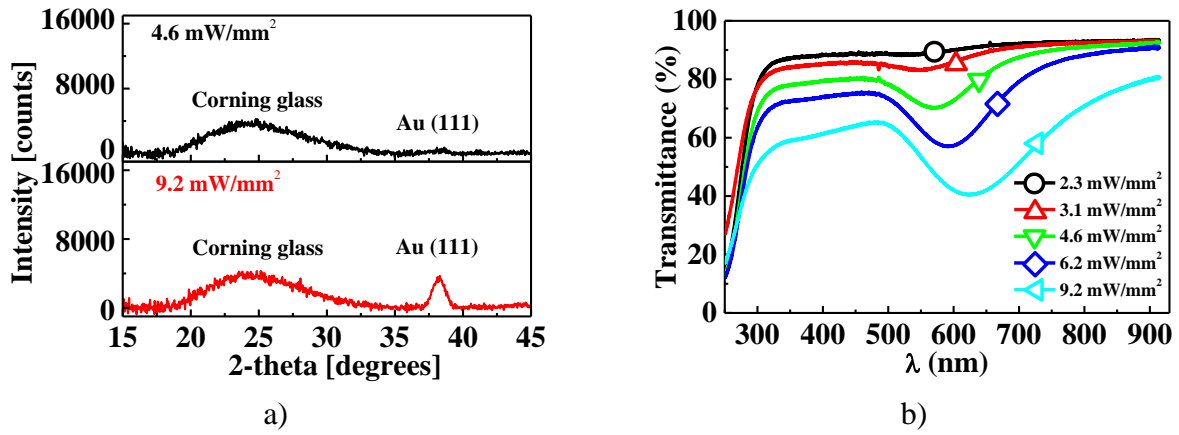


Figure 4.7 a) Examples of XRD lines of Au NIA sputtered on a Corning glass substrate at RF power densities of 4.6 mW/mm^2 and 9.2 mW/mm^2 ; b) transmittance spectrum of Au NIA on the Corning glass substrate (with RF power density as a parameter)

Au NIA sputtered on columnar ZnO:Al (Ga) thin films

Sequential sputtering Au NIA on AZO: Varying sputtering power

The morphology of the Au nanostructures formed on the ZnO:Al thin film was affected by the power density (2.3 to 18.5 mW/mm^2) as well as by the polycrystalline texture of the film surface (**Figure 4.8**). The modus of the Au nanostructure areas on the ZnO:Al thin film increased from 5 to 20 nm^2 , and the modus of the NN distance distribution changed from 4 to 9 nm (**Figure 4.9 a**).

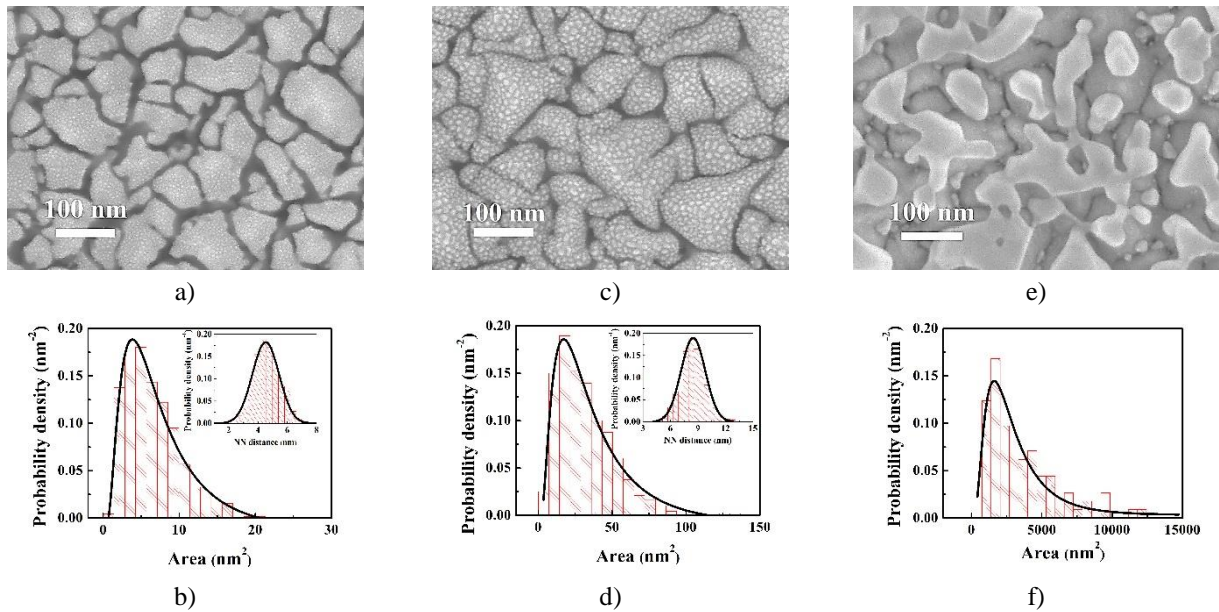


Figure 4.8 SEM images of Au nanostructures sputtered on ZnO:Al thin film/Corning glass substrate at varying ratios of power density/deposition rate/nominal thickness: a) $2.3 \text{ mW/mm}^2/0.12 \text{ nm s}^{-1}/1.1 \text{ nm}$; c) $4.6 \text{ mW/mm}^2/0.25 \text{ nm s}^{-1}/2.2 \text{ nm}$; e) $18.5 \text{ mW/mm}^2/1 \text{ nm s}^{-1}/9 \text{ nm}$; b), d), f) corresponding size and NN distance distributions of the Au nanostructures

The characteristic features of the morphology of RF diode sputtered Au nanostructures and some of their behaviours are comparable with the results obtained by DC diode sputtering [3,22]. The spectral optical transmittances of an uncoated ZnO:Al/Corning glass substrate

covered by Au at different power densities are shown in **Figure 4.9 b**. The range of power densities corresponded to the nominal thickness interval $1.1 \leq d_{\text{Au}} \leq 9$ nm. The transmittance of the ZnO:Al film/Corning glass substrate ($\sim 90\%$) decreased to $\sim 50\%$ with an increase in the sputtering power density (i.e. with the size of the Au nanostructure).

The minimum in the optical transmittance curves corresponds to the surface plasmon absorption [22] caused by the collective oscillation of electrons on the surfaces covered by Au nanostructures (**Figure 4.9 b**). The sputtering power density had an influence on the surface plasmon absorption wavelengths, which varied in the range 572 to 626 nm (corresponding plasmon resonant frequencies were 524 to 479 THz). The surface plasmon absorption peaks are characteristic of Au nanostructures. These results are in agreement with those for Au nanoparticles prepared by DC sputtering technologies [46]. The change in the shape of the plasmon absorption curves and the shift in the plasmon resonant frequencies with the sputtering power are caused by the different sizes of Au nanostructures and their various separations [22]. The red shift in the absorption minimum with an increase in the nominal thickness from 1.1 to 9 nm was not very strong, as reported in [3]. The use of thin film ZnO:Al underneath the Au nanostructures suppressed the LSPR (**Figure 4.9 b**), as the higher roughness of the ZnO:Al surface (in comparison with a glass surface) influenced this effect.

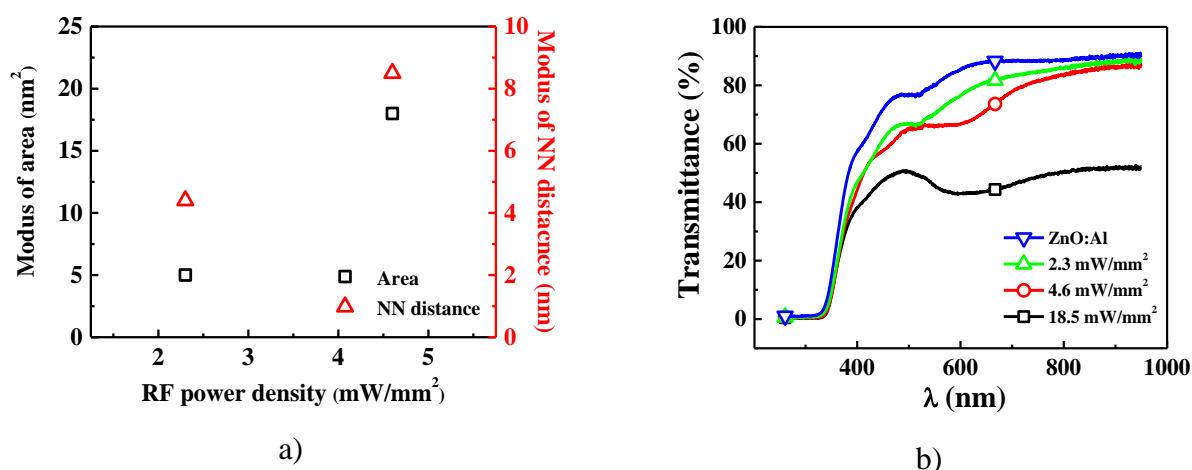


Figure 4.9 a) Modus of Au nanostructure areas and NN distance distribution sputtered on ZnO:Al/Corning glass; b) spectral transmittance of Au nanostructures sputtered at different power densities on a ZnO:Al/Corning glass substrate

Sequential sputtering of Au NIA on GZO substrate: Varying sputtering power

The application of LSPR sensors requires a solid transparent support, e.g. a glass substrate or TCO film. ZnO doped with Ga (GZO) belongs to the class of TCO films, which have attracted attention due to their nontoxic nature, cost-effectiveness and ease of fabrication [7]. We used the deposition concept of sequential (cyclic) sputtering. A Perkin/Elmer 2400/8L RF diode sputtering system was used for the deposition of GZO films and Au NIA on Corning glass substrates. The nominal thicknesses of Au island films (2-8 nm), sputtered from an Au target with diameter 203.2 mm at an RF power of 75–300 W, were determined by a Dektak profilometer. Post-deposition annealing was carried out in the sputtering chamber immediately after deposition (300°C/2 h).

SEM and the open source image processing program ImageJ [45] were used to evaluate the surface morphologies. A statistical analysis of SEM images of Au surface morphology (**Figure 4.10**) exhibited a log-normal distribution of the area of the NIA and a Gaussian distribution for the NN distance of the NIA.

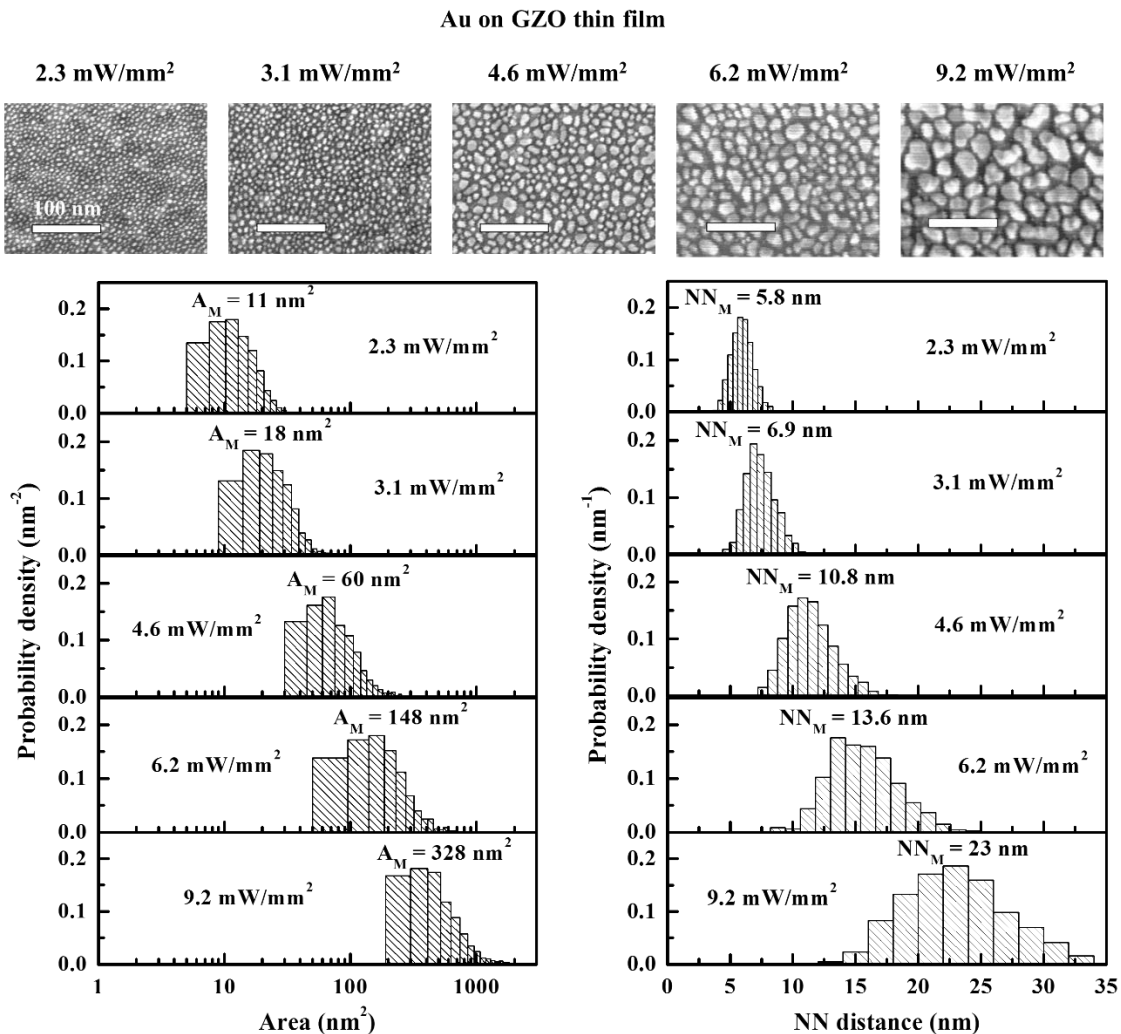


Figure 4.10 SEM images of Au nanoisland arrays sputtered on GZO thin film at different power densities/nominal thicknesses: 2.3 mW/mm²/2.4 nm, 3.1 mW/mm²/2.8 nm, 4.6 mW/mm²/3.8 nm, 6.2 mW/mm²/5.9 nm, and 9.2 mW/mm²/7.3 nm; statistical distribution of nanoisland areas and near neighbour distance (A_M and NN_M are the corresponding moduses)

An increase in the nominal thickness caused an evident increase in the nanoisland areas (diameters) (**Figure 4.10**), although their separations were extended only slightly. This varied between 11–328 nm² (GZO thin film/Corning glass substrate, **Figure 4.10**) depending on the RF sputtering power density. In both cases, the nanoisland NN distance exhibited a Gaussian distribution. We used very rough approximations to determine the nanoisland dimension D (assuming a circular shape for the NIA area ($D = 2 \cdot (\sqrt{A_M/\pi})$)) and inter-island separations s from the statistical evaluation of the SEM images ($s = NN_M - D$).

A comparison of NIA sizes leads us to the conclusion that the GZO thin film enhances the growth of nanoislands compared to those grown on the Corning glass substrate.

An XRD analysis indicates that the polycrystalline structure of Au NIA is preferentially oriented in the [111] direction (**Figure 4.11 a**). The texture of the Au NIA increased with the power density.

The transverse LSPR and the scattering were evaluated using transmission UV-Vis spectroscopy. The LSPR showed a red shift in the extinction peaks ($\Delta\lambda \leq 100$ nm) with an increase in the sputtering power density (**Figure 4.11 b**), giving rise to an increase in the size of the Au nanoislands. The results show that our optical measurements are limited regarding Au NIA sputtered at very low power densities. The minimum in the optical transmittance curves represents LSPR absorption corresponding to the extinction peak in the extinction spectra (where extinction is defined as a decadic logarithm of transmission). This phenomenon is the consequence of a collective oscillation of electrons in the Au NIA due to optical radiation. The coupled plasmon resonance wavelength λ depends on the nanostructure size, shape, orientation and local dielectric environment over the entire range of spectral regions from visible to NIR [24,47].

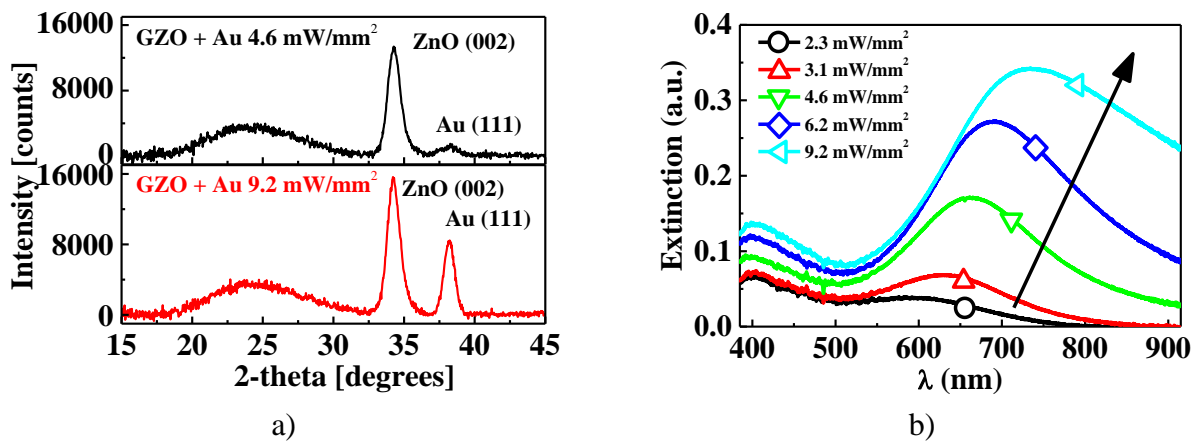


Figure 4.11 a) Examples of XRD lines of Au NIA sputtered on GZO/Corning glass substrate at RF power densities of 4.6 mW/mm^2 and 9.2 mW/mm^2 ; b) extinction spectrum of Au NIA on GZO thin film/Corning glass substrate (RF power density as a parameter)

Au NIA on a Ti-coated glass substrate

The specificity of the formation of nanostructures is highlighted here by exploiting the early stages of thin film growth. Sputtered non-continuous island Au films were grown according to the Volmer-Weber model [29]; **Figure 4.12** shows the formation of nuclei, clusters and islands and their coalescence.

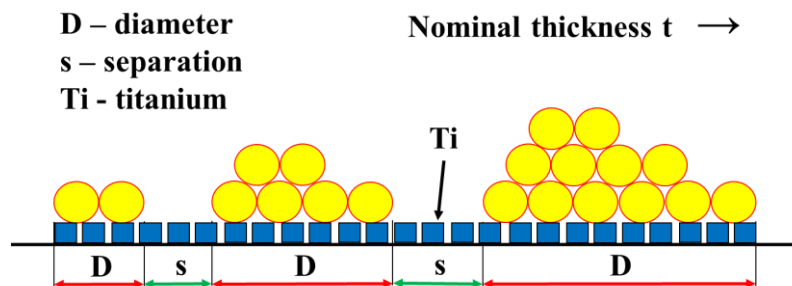


Figure 4.12 Schematic drawing of the Volmer-Weber model of film growth on a substrate, for a Ti layer that is not fully closed (orange rectangles represent the Ti layer)

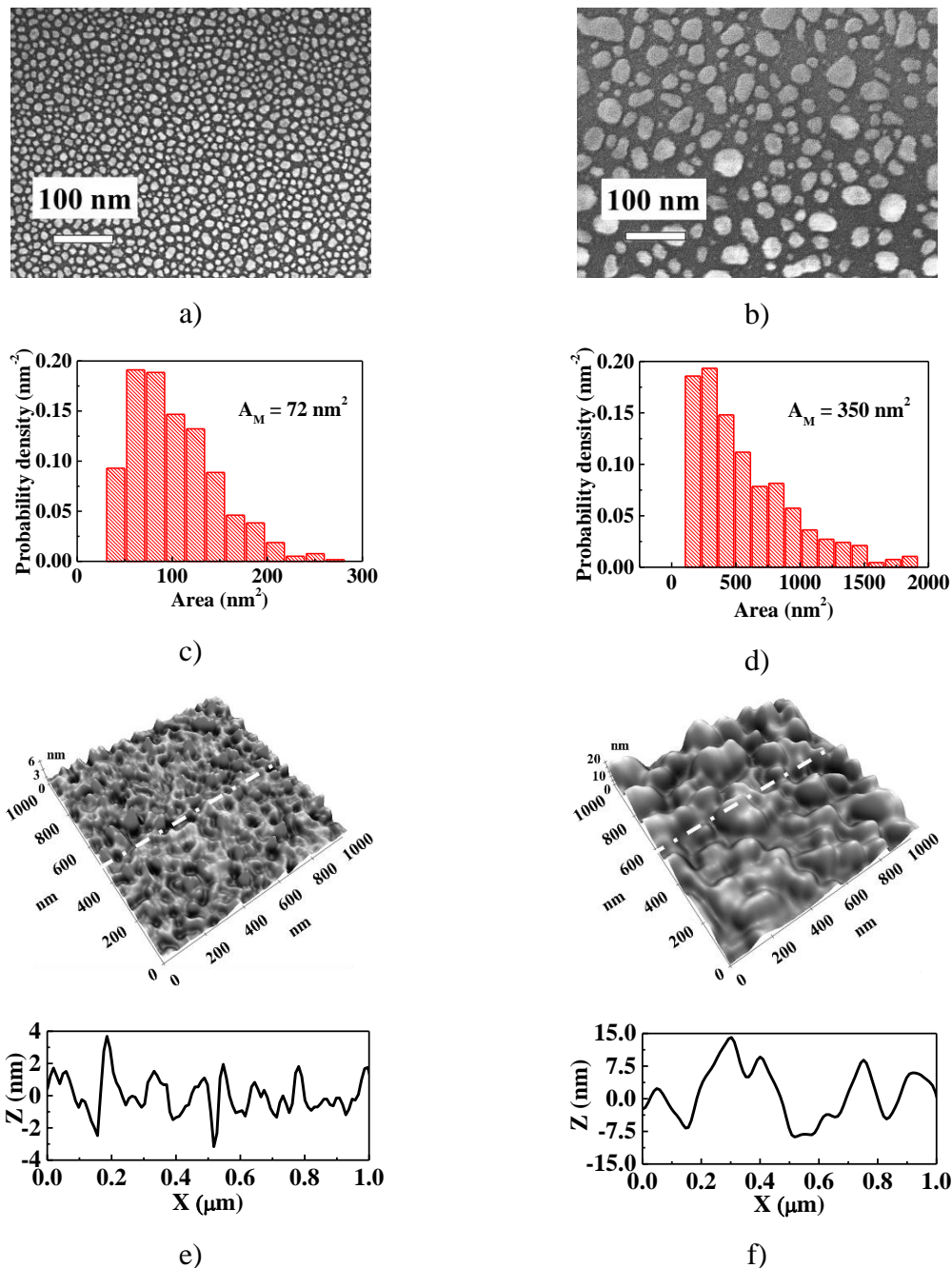


Figure 4.13 SEM images of Au nanoisland arrays after annealing in a vacuum, sputtered on a glass substrate: (a) with a non-continuous Ti film; (b) without Ti, using cyclic sputtering; (c, d) statistical analysis of surface morphology evaluated from SEM images; (e, f) AFM images of Au nanoislands with corresponding RMS profile

We sputtered Ti as an intermediate non-continuous film (approximately 0.6 nm in nominal thickness) on the glass substrate before gold sputtering, with the aim of improving the adhesion of the Au NIA. An Au NIA of the same nominal thickness of 6 nm was then sputtered on the glass (with or without Ti) at a power density of 2.3 mW/mm² and a substrate temperature of 200°C. After deposition, the substrates were immediately annealed in a vacuum at 300°C for 2 h (**Figure 4.13**). The adhesive non-continuous Ti film created very small “seeds” that can catch deposited Au atoms. After application of the Ti adhesive layer, the Au NIAs had a more uniform distribution; they were smaller, with a more defined shape (almost circular). The formation of more defined and well-dispersed Au/Ti NIA structures with smaller areas

($A_M = 72 \text{ nm}^2$, $s = 2.9 \text{ nm}$, $s/D = 0.31$) took place (**Figure 4.13 a, c**) compared to the single Au NIA ($A_M = 350 \text{ nm}^2$, $s = 5.9 \text{ nm}$, $s/D = 0.28$) (**Figure 4.13 b, d**). The positive effect of Ti upon the formation of stable Au NIA was also confirmed by AFM analyses (**Figure 4.13 e, f**) [26].

As a consequence, the scaling ratio s/D increased in the case of Au/Ti NIA, and a blue shift in the LSPR wavelengths was observed (**Figure 4.14**). The adhesive non-continuous Ti film caused only a small decrease in the intensity of the LSPR extinction spectra, compared to their significant broadening and intensity reduction due to the use of Ti or Cr adhesion layers with thicknesses of $\geq 1 \text{ nm}$ [48]. They were also more stable and relatively insensitive to temperature treatment. These aspects are advantageous for application of Au/Ti NIAs in LSPR biosensing.

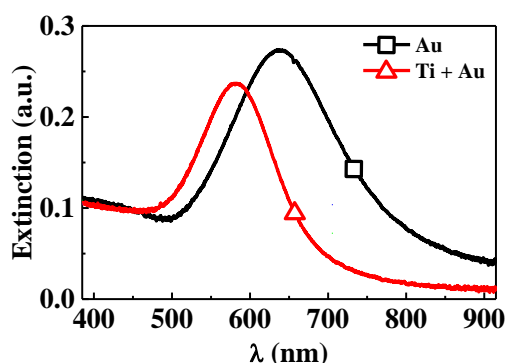


Figure 4.14 Extinction spectra for Au NIA sputtered on a glass substrate at 20°C with and without Ti after annealing in vacuum at 300°C for 2 h

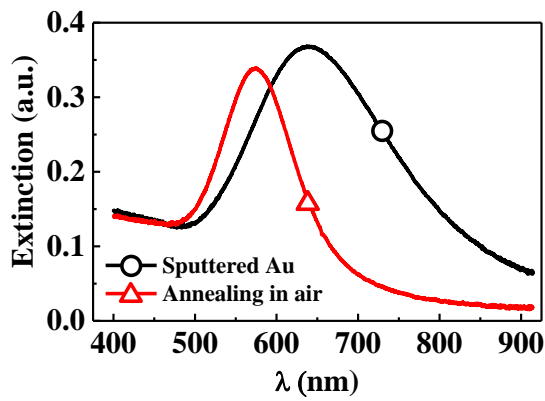
Study of annealing of Au NIA

Here, the annealing of ultra-thin Au films sputtered on glass substrates was investigated. The samples were annealed in air and in an evacuated chamber, and the dependence of the annealing process on the ambient pressure during thermal treatment was studied. Thermally induced changes in surface morphology were examined by AFM. These changes involve a high granularity of the surface morphology and coagulation of Au particles into larger aggregates, as confirmed by AFM analyses (**Figure 4.15 c, d**).

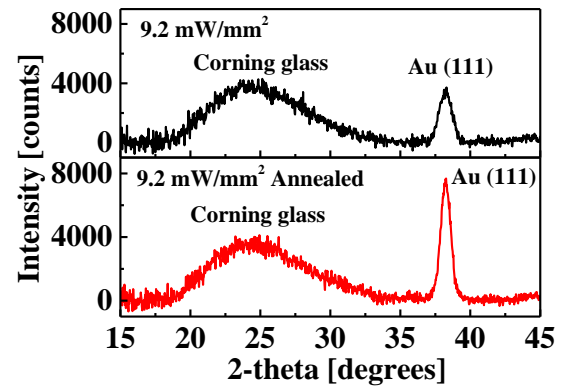
The energy delivery during the heat treatment had two main effects on the films: (i) growth of the gold nanoparticles due to coalescence (as clearly observed by AFM and SEM); and (ii) narrower widths of the X-ray diffraction line profiles, indicating higher dimensions of coherently diffracting domains (crystallites) and lower values of micro-strains. The heat treatment annealed several local structure imperfections within the crystallite volume for which the activation energies corresponded to the annealing temperatures used (**Figure 4.15 b**).

The structural and optical properties of the RF diode sputtered Au NIA were comparable to the results obtained by evaporation of ultrathin Au island films [20,21], RF diode sputtering of Au nanostructures [22], and cyclic sputtering and annealing of isolated/well-dispersed Au nanoisland arrays [23].

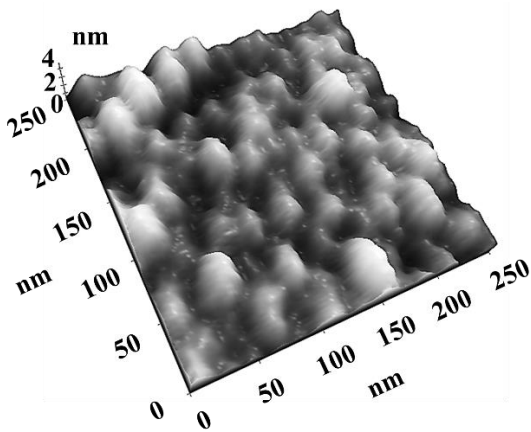
The thermal treatment of nanostructures after deposition is a well-known and important technological step in obtaining Au or Au/Ag nanoparticles of a particular size, shape and structure [17,20–22]. External annealing (500°C/5h in air) of our thicker Au NIA (thickness of 7.3 nm) had a significant effect on the morphology and LSPR. UV-Vis absorption spectra were used to investigate the optical parameters [22]. The extinction spectra exhibited an LSPR blue shift, $\Delta\lambda \leq -65 \text{ nm}$, after the annealing of Au NIA (**Figure 4.15 a**), due to the coalescence of small, closely spaced nanoislands.



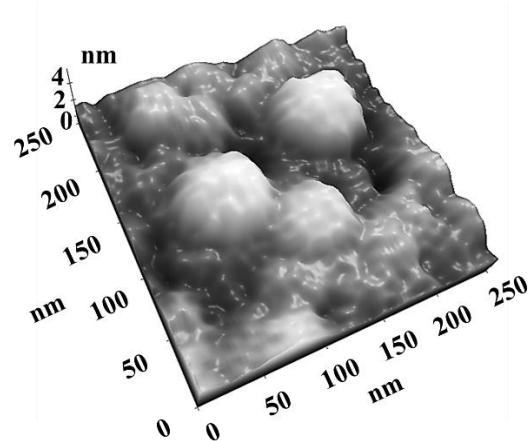
a)



b)



c)



d)

Figure 4.15 (a) Extinction spectra of Au NIA (7.3 nm in thickness) sputtered on Corning glass at 200°C before/after annealing in air; (b) XRD lines; corresponding AFM morphology (c) before and (d) after annealing of Au NIA

4.3 Universal size-scaling model for shift plasmon resonance

Comparison of plasmonic properties of Au NIA with universal size-scaling model for shift plasmon resonance wavelength

The structural, morphological and optical properties of sputtered Au nanoisland arrays (on Corning glass or GZO/Corning glass substrates) are studied and compared with the results of the universal size-scaling plasmon coupling model [24],[25]. A description of the plasmonic behaviour of sputtered Au NIA is also presented using technological parameters of thin films, such as the RF power density and the nominal thickness.

The LSPR showed a red shift in the extinction peaks ($\Delta\lambda \leq 100$ nm) with an increase in the sputtering power density (**Figure 4.16 a, b**, analysis the results from Chapter 4.2), giving rise to an increase in the size of the Au nanoislands.

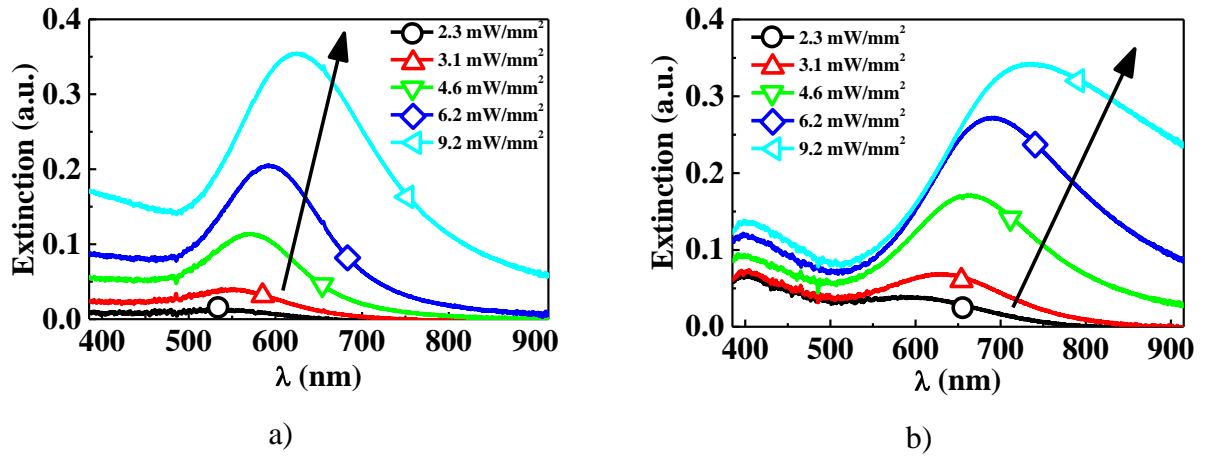


Figure 4.16 Influence of RF sputtering density on the extinction spectra of Au NIA sputtered on: (a) Corning glass substrate and (b) GZO thin film/Corning glass substrate

Our results are comparable to the universal size-scaling model of LSPR shift [47], where the fractional shift $\Delta\lambda/\lambda_0$ of the plasmon resonance wavelength varies with the ratio between the interparticle separation s and the particle dimension D . The s/D ratio characterises the inherent scaling of two competitive forces: the plasmon dipolar strength (polarisability) and the strength of the interparticle Coulombic restoring force. Based on these phenomena, the universal size-scaling plasmon rule equation was derived:

$$\frac{\Delta\lambda}{\lambda_0} = k \exp\left(-\frac{1}{\tau} \frac{s}{D}\right) \quad (1)$$

where $\Delta\lambda = \lambda - \lambda_0$ is the wavelength shift, λ_0 is the single-particle resonance wavelength for a very large s/D ratio, and $\tau \approx 0.2$ is the exponential decay constant.

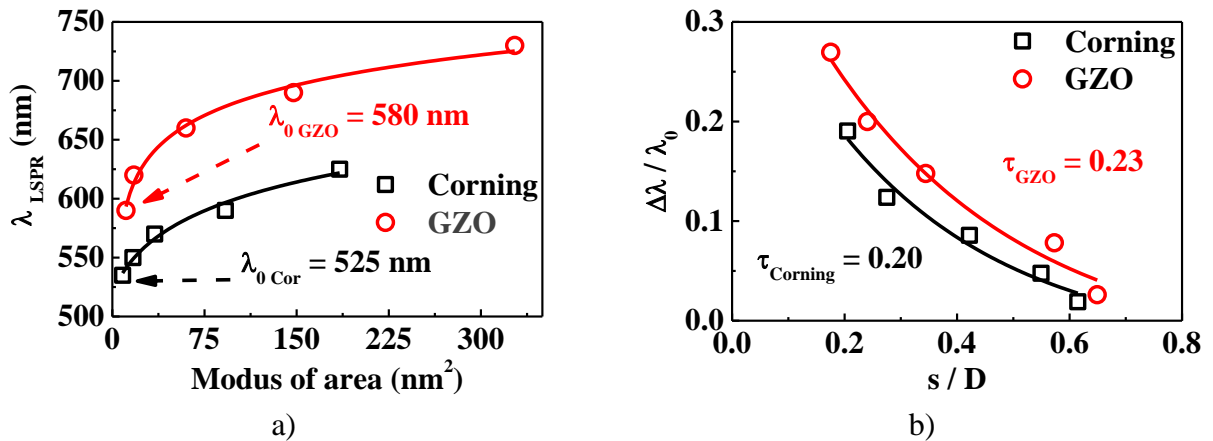


Figure 4.17 (a) Change in the plasmon resonance wavelength with A_M ; (b) the exponential dependence of the universal size-scaling rule (Equation 1) for NIA formed both on Corning glass and on GZO film substrates

The change in the plasmon resonance wavelength with the NIA A_M formed on Corning glass substrate and GZO film is shown in **Figure 4.17 a**. We define the reference resonant wavelength λ_0 as the minimum detectable value in our measurements.

Despite the arguments above, the fractional shift $\Delta\lambda/\lambda_0$ in the plasmon resonance wavelength showed an exponential dependence on the universal size-scaling rule for NIAs formed both on Corning glass and GZO film substrates (**Figure 4.17 b**). The decay constant τ was close to 0.2.

Modification of the universal size-scaling model of LSPR shift using a nominal thickness of Au film as a scale parameter

An attempt was then made to evaluate the LSPR response of Au NIA from the point of view of thin film technology. In our semi-empirical approach, the nominal thickness t was used for scaling. This implicitly characterises both the amount of deposited material and the distribution of the NIA (area/separation). Since the nominal thickness was linearly proportional to the RF power density (**Figure 4.5 a**), the curve of the LSPR wavelength versus the nominal thickness (**Figure 4.18 a**) showed the same form as the dependence of LSPR wavelength on the island area A_M (i.e. RF power density, **Figure 4.17 a**).

We therefore normalised the nominal thicknesses to the reference thickness t_0 corresponding to the reference resonant wavelength λ_0 as the minimum detectable value in our measurements. We found that the s/D ratio derived from the statistical evaluation of the SEM surface images was linearly proportional to the reciprocal thickness ratio t_0/t (**Figure 4.18 b**). This fact enabled us to replace the formal parameter s/D in Equation (1) by the ratio t_0/t , a phenomenological parameter that has no direct physical meaning in regard to the plasmon coupling strength.

The variation in the plasmon resonance wavelength fractional shift $\Delta\lambda/\lambda_0$ with the reciprocal relative thickness change t_0/t can then be described by the exponential dependence

$$\frac{\Delta\lambda}{\lambda_0} = k \exp\left(-\frac{1}{\tau_t} \frac{t_0}{t}\right) \quad (2)$$

where the constant τ_t mathematically describes the decay in the plasmon resonance wavelength fractional shift $\Delta\lambda/\lambda_0$ with nominal thickness (**Figure 4.18 c**).

In addition to the influence of another morphology, this comparison of NIAs formed on the glass or GZO film/glass substrates also demonstrates the refractometric effect of the substrate on the LSPR shift (**Figure 4.16 –Figure 4.18 a**). The refractive indices of Corning glass (≈ 1.5) and of GZO (≈ 2.0) are different, and this tends to shift the LSPR to longer wavelengths (including the reference single-particle resonance wavelength λ_0). This breaks the symmetry of the electromagnetic field distribution around the nanoisland (which is concentrated in the higher refractive index region), as confirmed both experimentally and by simulation [26,48].

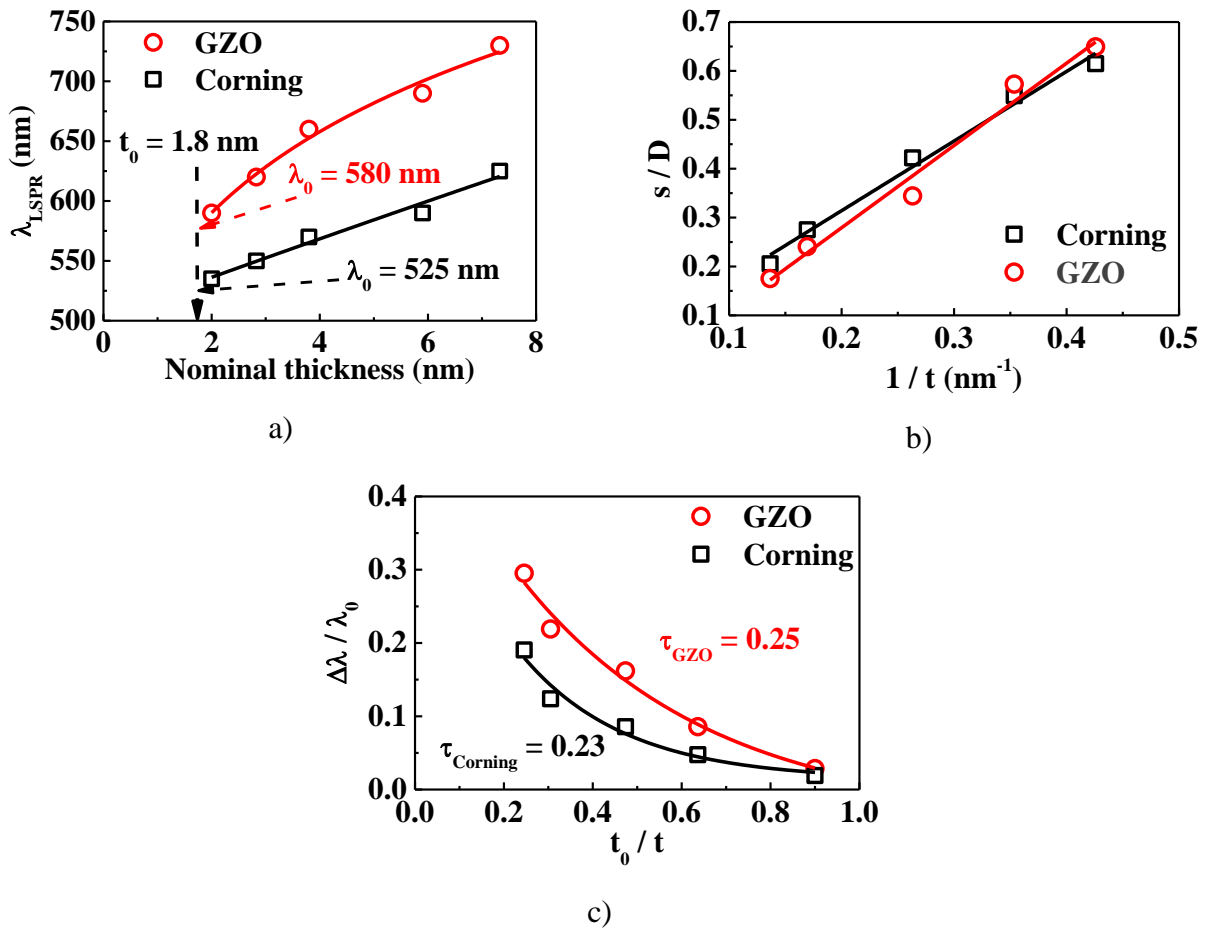


Figure 4.18 (a) Dependence of LSPR wavelength on (a) the nominal thicknesses of Au NIA sputtered on Corning glass/GZO thin film substrates; (b) relation between the scale factor s/D and the reciprocal thickness t_0/t of Au NIA; (c) exponential decay in the plasmon resonance wavelength fractional shift for NIA formed both on the Corning glass and GZO film/Corning glass substrates

4.4 Potential applications of Au NIA in bio-chemical optical sensorics

Bio-functionalisation of Au NIA/ZnO:Al surfaces and surface-enhanced raman spectroscopy study

Gold NIAs on ZnO:Al/Corning glass substrates were studied as plasmonic substrates for detection of the 11-mercaptoundecanoic acid (11-MUA) molecule in SERS, since this molecule is well known for its ability to bond to gold surfaces. The samples were transferred to a 11-MUA 2 $\mu\text{mol/ml}$ solution for 24 h to create a continuous 11-MUA monolayer on the sample surface. In order to remove the undesirable physically absorbed 11-MUA molecule, all samples were rinsed with ethanol and water and dried in nitrogen.

The SERS spectra of 11-MUA on Au nanostructures/ZnO:Al thin film as a function of different Au sputtering power densities are shown in **Figure 4.19**. The measured vibration bands of 11-MUA using Raman microscopy and their mode assignments can be attributed to bands which give information about the adsorption of 11-MUA on gold, surface $\nu(\text{C-S})$ gauche at 652 cm^{-1} , $\nu(\text{C-S})$ trans at 700 cm^{-1} , $\nu(\text{C-C})$ at 1058 cm^{-1} , vs (COO-Au) at 1394 cm^{-1} . Both of the

apparent assignments of $\nu(\text{C-S})\text{T}$ and $\nu(\text{C-C})$ give information about the conformational state of the adsorbed molecule on the gold surface, showing the trans nature of the adsorbed molecule. It was also observed that the peak intensity of adsorbed 11-MUA on Au nanostructures, when exposed to 9 mW/mm^2 power density, is significantly superior to that of other exposed substrates (**Figure 4.19**). It is well known that the Raman signal strength is proportional to the power of the Raman laser exciting the sample. In our case, a decrease in the intensity of the major Raman peaks was observed even when the laser power was increasing. This can be explained by the occurrence of damage to the sample with the increase in laser power. It was also observed that the substrate without Au nanostructures did not show the specific Raman bands of the organic molecule. Significant enhancements are obtained when an organic molecule is adsorbed on a nanostructured substrate such as Au, Ag or Pt, [5,46,49–52].

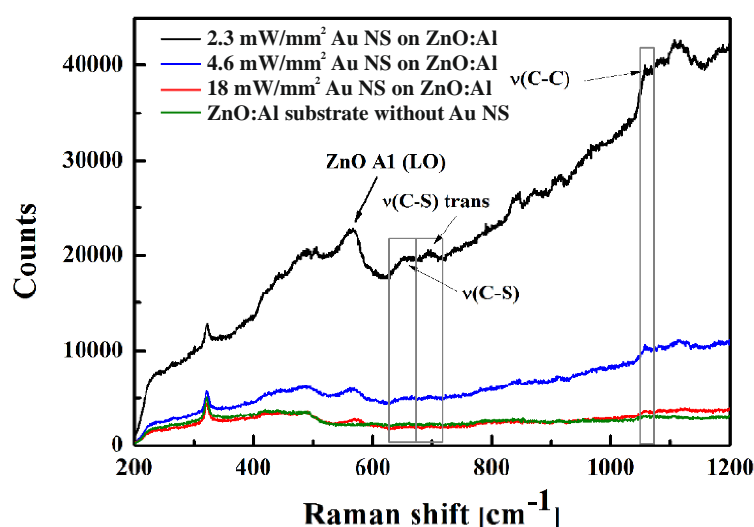


Figure 4.19 SERS spectra of 11-MUA on Au nanostructure/ZnO:Al thin film at different Au sputtering power densities

Optical refractive LSPR sensing of bio-functionalised Au nanoislands

The sensitivity of plasmonic nanosensors is particularly influenced by sensing based on both plasmon coupling and target-induced local refractive index changes. The first effectively improves the detection sensitivity by increasing the size of the aggregates and decreasing the distance between them. According to the universal size-scaling model of LSPR shift [25] the fractional shift $\Delta\lambda/\lambda_0$ of the plasmon resonance wavelength varies with the ratio of the interparticle separation s and the particle dimension D . We used very rough approximations to determine the nanoisland dimension D (assuming a circular shape of the nanoisland area, $D = 2 \cdot (\sqrt{A_M/\pi})$) and inter-island separation s from the statistical evaluation SEM images ($s = NN_M - D$). NN_M is modus of the NN distance of NIA. The intermediate ultrathin non-continuous sputtered Ti film (with a nominal thickness of 0.6 nm) acts as a “seed” for Au growth on the Corning glass substrate. This can improve the adhesion of Au NIA and support the formation of more defined Au/Ti NIA structures of smaller dimensions (modus of island size $D = 10 \text{ nm}$ and $s = 2 \text{ nm}$, **Figure 4.20 a**) in comparison with the Au NIA itself ($D = 16 \text{ nm}$, $s = 8 \text{ nm}$, **Figure 4.20 b**).

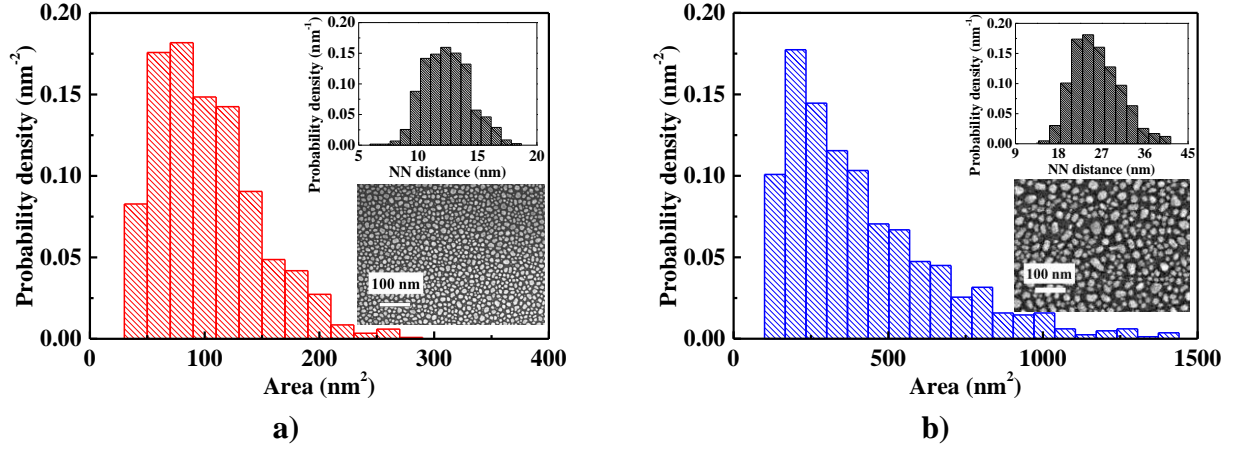


Figure 4.20 SEM images of (a) Au/Ti and (b) Au NIA of nominal thickness $t \approx 5$ nm

The LSPR wavelength blue shift $\Delta\lambda = -21$ nm corresponded to the lower dimensions of the Au/Ti NIA, and is in agreement with the universal size-scaling model for LSPR [25].

Refractive index-based (refractometric) sensing offers several advantages, such as the possibility of miniaturisation, compatibility with microfluidics and a broader range of available functionalisation chemistry [48]. The specific properties of this sensing include small size nanoparticles with high absorption ratios, while larger nanoparticles have high scattering ratios; in addition, anisotropic shape nanostructures exhibit a higher refractive index sensitivity than spherical nanoparticles. The LSPR wavelength shift $\Delta\lambda$ in response to changes in refractive index is approximately described as follows:

$$\Delta\lambda \approx m (n_{\text{adsorbate}} - n_{\text{medium}})(1 - e^{-2d/l_d}) \quad (3)$$

where m is the sensitivity factor (in nm per refractive index unit (RIU)); $n_{\text{adsorbate}}$ and n_{medium} are the refractive indices (in RIU) of the adsorbate and medium surrounding the nanoparticle, respectively; d is the effective thickness of the adsorbate layer (nm); and l_d is the electromagnetic field decay length (nm) [48].

The self-assembly of a 11-MUA monolayer on surfaces of Au NIA induced a different LSPR wavelength shift depending on the size of the Au nanoislands (their nominal thickness t).

Smaller NIA structures with nominal thicknesses of 5 nm (**Figure 4.20**) showed small LSPR blue shifts of $\Delta\lambda = -11$ nm (Au NIA) and $\Delta\lambda = -13$ nm (Au/Ti NIA) after modification by 11-MUA (**Figure 4.21 a**). This was probably caused by the formation and local polarisation of an 11-MUA monolayer (with thickness about 1 nm) only on individual Au islands. This reduces the plasmon coupling strength among nanoislands, thus inducing a blue shift in the LSPR wavelength according to the universal size-scaling model [25]. When the Au NIA was thicker (thickness of 16 nm), the nanoislands were larger ($D = 21$ nm) and their separations lower ($s = 6$ nm), as shown in **Figure 4.21 b**. The coverage of 11-MUA was then approximately continuous, and we could expect the refractive index-based sensing to be dominant. All optical measurements were performed in air ($n_{\text{medium}} = 1$). The red shift in the LSPR wavelength was observed to be $\Delta\lambda = +24$ nm, and this is in agreement with empirical and theoretical expectations (the refractive index of MUA is $n_{\text{adsorbate}} \approx 1.5$) [53], **Figure 4.21 b**. Sputtered NIAs with higher thicknesses of > 10 nm can exploit the specific properties of refractive index-based sensing [54]: smaller nanoparticles have higher absorption ratios, while larger nanoparticles have

high scattering ratios. Anisotropic shape nanostructures also exhibit higher refractive index sensitivities than spherical nanoparticles [55].

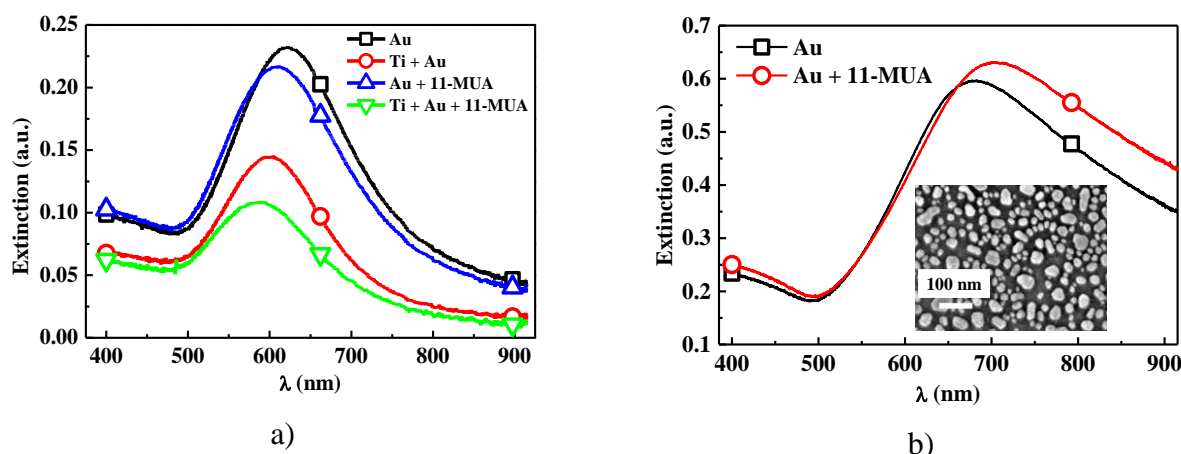


Figure 4.21 Blue shift in the LSPR wavelength corresponding to lower dimensions of the Au/Ti NIA (\circ) in comparison with Au NIA (\square). Influence of 11-MUA coverage on extinction spectra (LSPR wavelength shift) of (a) Au (Δ) or Au/Ti NIA (∇) of nominal thickness $t = 5$ nm; (b) Au NIA (\circ) of $t = 16$ nm (SEM image is inserted)

Electrochemical impedance spectroscopy study of Au NIA-coated Pt interdigital array of electrodes

A set of experiments were carried out using interdigital microelectrode arrays (IDEA). Here, the $10\ \mu\text{m}/10\ \mu\text{m}$ (width and gap) IDEA was made from platinum, and the gold nanoislands were sputtered on these IDEAs using RF diode sputtering, as described above (Figure 4.22).

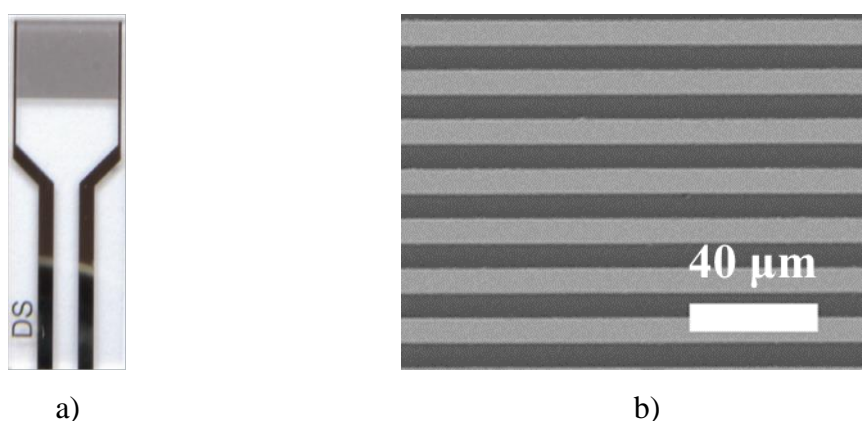


Figure 4.22 Interdigitated platinum electrodes (IDAEs) from Dropsens ltd. (Spain): (a) photo of the sensor; (b) SEM images of $10\ \mu\text{m}$ IDEA; (c) AFM image of the structure

Here, impedance spectroscopy was used for the detection of trisodium citrate. Trisodium citrate is used as an anticoagulant in blood transfusions (the citrate ion chelates the Ca ions in the blood by forming Ca citrate compounds, disrupting the aggregation of erythrocytes) and as a food additive for flavouring or a preservative (E331).

Trisodium citrate ($\text{Na}_3\text{C}_6\text{H}_2\text{O}_7$) concentrations in the range 0.01–0.5 mM were evaluated using electrochemical impedance spectroscopy (EIS), with an IDAE microsensor consisting of Pt IDAE, and AuNIA with and without Ti film, respectively (**Figure 4.23**).

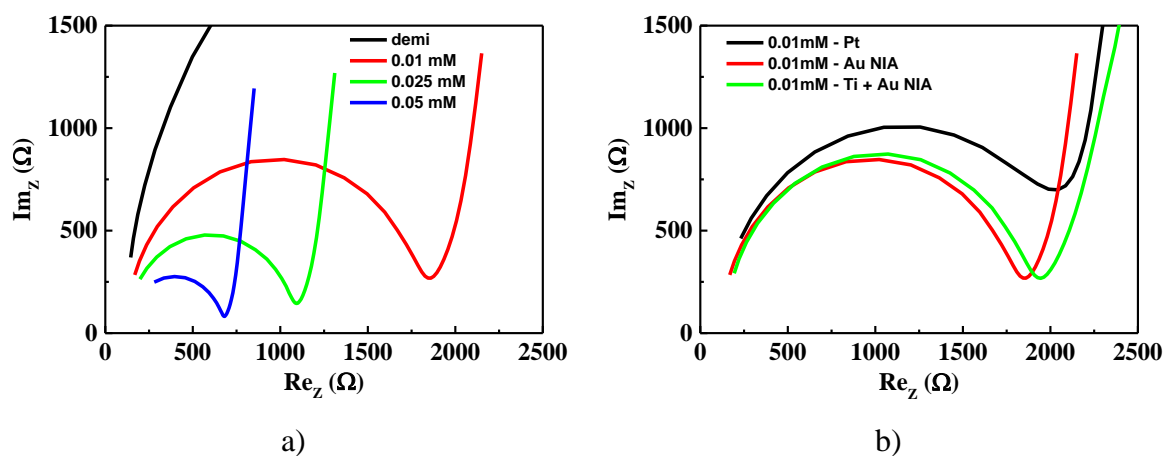


Figure 4.23 Electrochemical impedance spectroscopy of trisodium citrate (a) at different concentrations with a Pt IDT electrode and Au NIA; b) comparison of Pt electrode and Au NIA, with and without Ti

The advantage of EIS is that it provides a comprehensive description of the electrochemical behavior of the investigated system. A small excitation will only cause a small "irritation" of the studied system, and this can reduce the errors arising from the measurement technique. By introducing a small change in the potential, the existing characteristics of the system of electrode cells do not change, including no change its direction. The results of measurement simultaneously include both faradaic and non-faradaic phenomena, meaning that it is possible to obtain information from the EIS about the mechanism of the ongoing electrochemical processes. Since this method does not involve a change in the potential during measurement, direct current potential problems arise with potential control in the low conductivity solutions.

The results of EIS measurement correspond to an equivalent electrical circuit (system model) including parameters such as the solution resistance, double layer capacity, etc. The simplest model is the Randles electrochemical cell, for which the function core is a parallel combination of a capacitor and resistor (**Figure 4.24**) [56].

The figure below shows a representative Nyquist graph for a Randles cell. At high frequencies, the capacitor acts as a conductor, and the total impedance is given only by the resistor R_s . At low frequencies, the capacitor behaves as an insulator, and the total impedance is then given by the sum of resistors R_s and R_{ct} . Changes in the conductivity of the solution (R_s) cause a shift of the curve along the x-axis. A change in the hub resistance (R_{ct}) changes the shape of the curve (for a Randles cell, this is exactly a semicircle). The change in capacity is reflected in the Nyquist graph by changing the distribution of points to a semi-circle. If the capacity is too high, all the points in the first half, i.e. the semicircle, are not complete. Similarly, for a capacity that is too low, the first part of the semicircle is missing (again only in Randles cells). In order to compare the results, we use a replacement circuit with a fitted function.

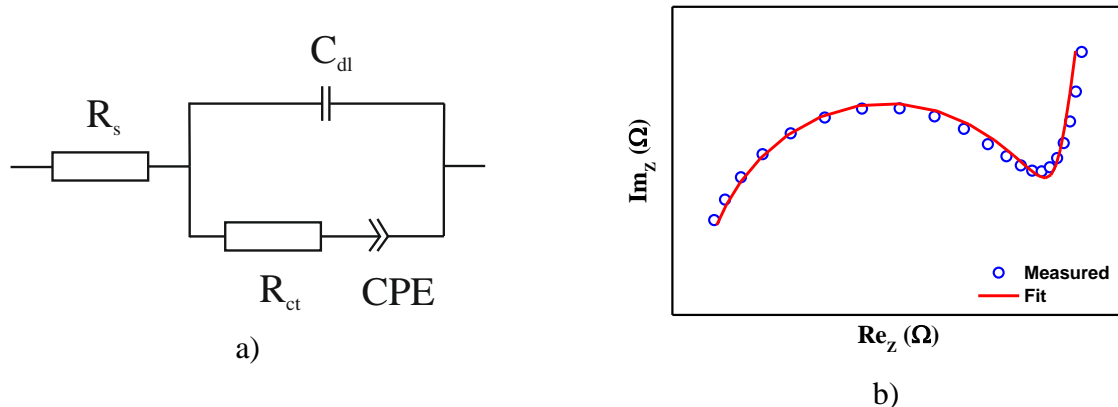


Figure 4.24 (a) Replacement circuit; and (b) the fitted curve for a schematic diagram of a Randles cell equivalent electric circuit, where R_s is the resistivity, R_{ct} represents the charge resistance and the C_{dl} corresponds to the capacity of the electrical double layer. The Nyquist graph is shown for a Randles cell, with fitting of measured results [56].

5 Conclusion

The main contributions of the dissertation can be summarised as follows:

- 1) The results of our research confirm the particular advantage of sputtering in preparing AZO films with a nanocolumnar polycrystalline structure. The most significant deposition parameter was the substrate temperature (about 200°C), which primarily influenced the crystalline structure. The aim of our research was the development of Au nanoisland arrays (Au NIA) for sputtering technology, without use of additional patterning methods.
 - a) A sequential sputtering technology was developed for the formation of transparent and conductive very thin AZO films (with thickness ≈ 100 nm) which exhibited (in comparison with the continuous deposition mode): (i) a substantial nanocolumnar (002) texture containing highly ordered crystalline grains (crystallite sizes $\langle D_c \rangle \approx 65$ nm); (ii) low lattice stress gradients ($\approx 10^{-2}$ – 10^{-1} GPa/nm) and microstrains ($\langle \varepsilon \rangle \approx 7 \times 10^{-3}$); (iii) comparable resistivities ($\approx 10^{-1}$ Ωcm); (iv) high optical transparency (≈ 90 %); and (v) an adequate refractive index (≈ 2.0).
 - b) Particular features of sequential sputtering included a low deposition rate (on the order of 0.1 nm/s) and a more or less isotropic deposition at working gas pressures of 1 Pa or above; this opens the way to use this approach in the controllable nanocoating of 3D samples, as proven by the sputtering of a highly consistent coverage (shell) of GaP nanowires [28,38].
 - c) The results presented here verified the potential for the use of nanocolumnar structures of ZnO for biochemical sensing applications due to their large surface-to-volume ratio and chemically active surface facets.
- 2) We developed technological procedures for the formation of Au plasmonic nanostructures (island-like shape) directly by sputtering, without masking and lithography:
 - a) The specificity of the formation of Au sputtered NIAs on a glass substrate or on a ZnO thin film doped by Ga was ascertained. A statistical analysis of morphology images (SEM, AFM) showed a log-normal distribution of the size (area) of nanoislands. The

- modus A_M varied from 8 to 328 nm² depending on the sputtering power density, which determined the nominal thickness in the range 2 to 15 nm. The preferential polycrystalline texture (111) of Au NIA increased with the power density and after annealing.
- b) Transverse LSPR (evaluated by transmission UV/Vis spectroscopy) showed a red shift in the extinction peaks ($\Delta\lambda \leq 100$ nm) with an increase in the nominal thickness and a blue shift ($\Delta\lambda \leq -65$ nm) after annealing of Au NIAs.
 - c) The plasmonic behaviour of Au NIAs was described by modification of a size-scaling universal model, using the nominal thin film thickness as a technological scaling parameter.
 - d) Sputtering of an intermediate adhesive ultrathin Ti film between the glass substrate and the gold improves the adhesion of Au nanoislands, and supports the formation of more defined Au NIA structures with smaller dimensions.
- 3) The potential application of Au NIAs in biochemical sensors was demonstrated. For bio-functionalisation of Au NIA surfaces, we used 11-MUA, which improves the attachment of biomolecules such as proteins and antibodies:
- a) The self-assembly of 11-MUA monolayers at Au NIA surfaces formed on ZnO:Al thin film was investigated using SERS. The measured vibration Raman bands of 11-MUA and their mode assignments confirmed the immobilisation of 11-MUA on gold nanostructures.
 - b) The use of sputtered Au NIA in the development of refractometric LSPR biosensors was demonstrated. The self-assembly of 11-MUA monolayers induced a blue or red shift in the LSPR wavelength depending on the size of the Au NIAs (their nominal thickness).
 - c) Trisodium citrate ($\text{Na}_3\text{C}_6\text{H}_2\text{O}_7$) concentrations in the range 0.01–0.5 mM were evaluated using EIS with an IDAE microsensor consisting of Pt IDAE and Au NIA. Trisodium citrate is used as an anticoagulant in blood transfusion (the citrate ion chelates the Ca ions in the blood by forming Ca citrate compounds disrupting the erythrocytes aggregation), as a food additive for flavouring, or as a preservative (E331).

6 Resumé

Tenká vrstva sa môže charakterizovať ako "dvojrozmerná" štruktúra, pretože hrúbka tretieho rozmeru je taká malá (od 1 μm do 1 nm), že pomer povrchu k objemu je pomerne veľký (až 10^6). Zníženie vzdialenosti medzi dvoma povrchmi a ich interakcia má rozhodujúci vplyv na vnútorné fyzikálne a chemické vlastnosti tenkých vrstiev a vedie k vzniku úplne nových javov. Zmeny v kryštalickej štruktúre a v chemickom zložení takisto spôsobujú, že vlastnosti tenkých vrstiev sú veľmi rozdielne a môžu sa výrazne líšiť od objemových materiálov. Vo všeobecnosti tenké vrstvy vytvárajú "most" medzi makro a nano systémami a vývoj a výroba moderných mikrosenzorov sa nedá dosiahnuť bez použitia technológií tenkých vrstiev.

Táto práca sa zameriava na kombináciu tenkých vrstiev ZnO a nanoštruktúr Au. ZnO dopovaný s Al (ZnO:Al) alebo Ga (ZnO:Ga) patrí do skupiny tenkých vrstiev transparentného vodivého oxidu (TCO); tieto majú špecifické elektronické a optické vlastnosti, ktoré sú

použiteľné v solárnych článkoch, optoelektronike a senzoch. Z nanoštruktúrovaných vzácnych kovov má Au osobitný význam vďaka svojej stabilite a jedinečným elektrochemickým a optickým vlastnostiam. Morfológia povrchu Au je vlastnosť, ktorá najviac ovplyvňuje jeho funkčné vlastnosti. Au nanoštruktúry sa často pripravujú metódami elektrochemickej depozície, ale existuje niekoľko správ o naprašovaných mikro a nano štruktúrach. Výskum Au nanoštruktúr naprášených na sklenené a stĺpcové TCO tenké vrstvy je dôležitý, pretože výsledky sú použiteľné pre biochemické senzory.

Hlavným cieľom dizertačnej práce bude získanie nových poznatkov pri technológii prípravy a charakterizácii sensorických rozhraní/povrchov na báze tenkých/ultratenkých vrstiev ZnO a nanoštruktúr Au, t. zn. prispieť ku poznaniu základných súvislostí medzi štruktúrou/morfológiou týchto systémov a ich vybranými fyzikálnymi, chemickými i elektrochemickými vlastnosťami.

Tézy dizertačnej práce sú zhrnuté v nasledujúcich bodoch:

1. Vyvinúť efektívne technológie vysokofrekvenčného naprašovania a tepelného žihania pre prípravu:
 - a) transparentných vodivých oxidových (TCO) tenkých vrstiev ZnO dopovaných Al (ZnO:Al) alebo Ga (ZnO:Ga) s nanostĺpikovou kryštalickou štruktúrou,
 - b) Au nano- častíc/štruktúr bez fotolitografického tvarovania, vhodných pre transparentné sensorové štruktúry, prípadne pre fotovoltaické solárne články.
2. Rozšíriť znalosti o fyzikálno-chemických vlastnostiach nanoštruktúrovaných rozhraní na báze TCO ZnO vrstiev a Au nano- častíc/štruktúr pomocou ich charakterizácie analyzačnými metódami: povrchov (hrúbka, mikrodrsnosť – Dektak, morfológia – SEM, AFM), kryštalickej štruktúry (XRD), elektrických parametrov (rezistivita, koncentrácia a pohyblivosť nosičov náboja – Hall/Van der Pauw merania), optickej spektrometrie (absorpcia, UV/VIS/IR / Ramanova spektroskopia), electrochémie (voltampérometria / impedimetria).
3. Riešiť špeciálne kvantitatívnu analýzu SEM zobrazenie morfológie povrchu nanoštruktúrovaných ZnO tenkých vrstiev ako aj Au nano- častíc a nano-štruktúr.
4. Pripraviť naprašované Au fotonické štruktúry využívajúce plazmónovú rezonanciu a vykonať ich optické predbežné testovanie v niektorých zvolených biochemických analýzach.

Účelom tejto práce bolo vyvinúť, študovať a optimalizovať technológiu, ktorá vedie k tvorbe Au nanoštruktúr na tenkých vrstvách TCO ZnO:Al (ZnO:Ga) alebo sklenených substrátoch. Táto práca je preto rozdelená do niekoľkých kapitol, ktoré sa zameriavajú na tieto oblasti:

- (i) Štúdium naprašovania nanostĺpikových tenkých vrstiev ZnO:Al a ich komplexná charakterizácia (t.j. ich povrchová morfológia, kryštalická štruktúra, elektrická a optická charakterizácia);
- (ii) Štúdiá vplyvu výkonu rádiových frekvencií (RF) diódového naprašovania na morfológiu ultratenkých vrstiev Au deponovaných na tenkých vrstvách ZnO:Al (ZnO:Ga) alebo sklenených substrátoch;
- (iii) Štúdiá absorpcie povrchových plazmonických Au nanoštruktúr vytvorených na substrátoch zo skla alebo ZnO:Al (ZnO:Ga); a

- (iv) Štúdiá povrchovej absorpcie Ramanovej spektroskopie (SERS) Au nanoštruktúr vytvorených na ZnO:Al substrátoch funkcionalizovaných kyselinou 11-merkaptoundekanovou (11-MUA).

Práca prispieva k vývoju jednoduchých a účinných technológií naprašovania a tepelného žihania na prípravu transparentných vodivých oxidov ZnO:Al alebo ZnO:Ga tenkých vrstiev s nanostĺpikovými štruktúrami a Au plazmonickými nanočasticami a nanoštruktúrami s minimálnym fotolitografickým spracovaním. Táto štúdiá rozšíri existujúce poznatky o fyzikálno-chemických vlastnostiach nanoštrukturovaných rozhraní medzi dopovanými vrstvami ZnO a Au nanoštruktúrami prostredníctvom komplexnej štúdie využívajúcej komplexné techniky charakterizácie.

Hlavné prínosy dizertačnej práce je možné zhrnúť nasledovne:

- 1) Výsledky nášho výskumu potvrdzujú obzvlášť výhodu naprašovania pri príprave tenkých vrstiev oxidu zinočnatého (AZO) s nanostĺpikovou polykryštalickou štruktúrou. Najvýznamnejšími parametrami naprašovania boli rýchlosť depozície (v ráde 0.1 - 1 nm/s) a teplota substrátu (približne 200 °C), ktorá primárne ovplyvnila kryštalickú štruktúru. Cieľom nášho výskumu bolo vývoj Au nanoostrovčekových polí (Au NIA) pre technológiu naprašovania bez použitia ďalších formovacích metód.
 - a) Sekvenčná (cyklická) naprašovacia technológia bola vyvinutá pre tvorbu transparentných a vodivých veľmi tenkých vrstiev AZO (o hrúbke ≈ 100 nm), ktoré vykazovali (pri porovnaní s metódou kontinuálnej depozície): i) výraznú nanostĺpikovú (002) štruktúru obsahujúce vysoko usporiadané kryštalické zrna (veľkosť kryštálov $\langle D_c \rangle \approx 65$ nm); ii) nízky gradient namáhania mriežky ($\approx 10^{-2}$ - 10^{-1} GPa / nm) a mikroštruktúry ($\langle \varepsilon \rangle \approx 7 \times 10^3$); iii) porovnateľná rezistivita ($\approx 10^{-1}$ Ω cm); iv) vysoká optická transparentnosť ($\approx 90\%$); a v) adekvátni index lomu ($\approx 2,0$).
 - b) Konkrétne vlastnosti sekvenčného naprašovania zahrňujú nízku depozičnú rýchlosť (rádovo 0,1 nm/s) a viac alebo menej izotropnú depozičnú rýchlosť pri tlakoch pracovného plynu 1 Pa alebo vyššie; to otvára spôsob, ako tento prístup využívať pri kontrolovateľnom nanopokrývaní 3D vzorkov, ako dokazuje naprašovanie vysoko konzistentného pokrytia (jadro) nanodrôtov GaP.
 - c) Tu uvedené výsledky overili potenciál pre použitie nanostĺpikových štruktúr ZnO pre aplikácie biochemickej detekcie vďaka ich veľkému pomeru povrchu k objemu a chemicky aktívnym povrchovým plochám.
- 2) Vyvinuli sme technologické postupy pre tvorbu Au plazmonických nanoštruktúr (ostrovčekového tvaru) priamo naprašovaním bez maskovania a litografie:
 - a) Bola zistená špecifická tvorba naprášených Au NIA na sklenenom substráte alebo na tenkej vrstve ZnO dopovaného Ga. Štatistická analýza morfológických obrázkov (SEM, AFM) ukázala log-normálne rozdelenie veľkosti (plochy) nanoostrovčekov. Modus A_M sa pohyboval od 8 do 328 nm² v závislosti na hustote naprašovacieho výkonu, ktorá určovala menovitou hrúbku v rozmedzí 2 až 15 nm. Preferenčná polykryštalická štruktúra (111) Au NIA sa zvýšila s hustotou výkonu a žihania po depozičii.

- b) Transverzálna LSPR (vyhodnotená transmisnou UV/Vis spektroskopiou) vykazuje červený posun v extinkčných vrcholoch ($\Delta\lambda \leq 100$ nm) so zvýšením nominálnej hrúbky a modrým posunom ($\Delta\lambda \leq -65$ nm) po žíhaní Au NIAs.
 - c) Plazmonické správanie Au NIA bolo popísané modifikáciou univerzálneho modelu posunu plazmonickej frekvencie založený na veľkostnej mierke, s použitím nominálnej hrúbky tenkej vrstvy ako parameter technologickej mierky.
 - d) Naprašovanie strednej adhéznej ultratenkej vrstvy Ti medzi sklenený substrát a Au zlepšuje priľnavosť Au nanoostrovčekom a podporuje vytváranie lepšie definovaných štruktúr Au NIA s menšími rozmermi.
- 3) Bola ukázaná potenciálna aplikácia Au NIA v biochemických senzoch. Pre bio-funkcionalizáciu povrchu Au NIA sme použili 11-MUA, ktorá zlepšuje pripojenie biomolekúl, ako sú proteíny a protilátky:
- a) Vlastná zostava 11-MUA monovrstiev na povrchu Au NIA vytvorených na tenkej vrstve ZnO:Al bola skúmaná pomocou SERS. Namerané vibračné Ramanove pásma 11-MUA a k nemu priradené módy potvrdili imobilizáciu 11-MUA na Au nanoštruktúrach.
 - b) Bolo preukázané použitie naprašovania Au NIA vo vývoji refraktometrických biosenzorov LSPR. Vlastné zostavenie 11 monovrstiev MUA vyvolalo modré alebo červené posuny vo vlnovej dĺžke LSPR v závislosti na veľkosti Au NIA (ich nominálna hrúbka).
 - c) Koncentrácie citrátu trisodného ($\text{Na}_3\text{C}_6\text{H}_2\text{O}_7$) v rozmedzí 0,01 až 0,5 mM boli vyhodnotené pomocou EIS s IDAE mikrosenzorom pozostávajúcim z Pt IDAE a Au NIA. Citrát trisodný sa používa pri krvnej transfúzii a dialýze ako antikoagulant (citrátový ión naviaže Ca ióny v krvi tým, že vytvára Ca citrátové zlúčeniny, ktoré narušujú agregáciu erytrocytu), ako aj potravinárska prídavná látka k aromatizácii alebo ako konzervačná látka (E331).

7 References

- [1] J. Elias, M. Gizowska, P. Brodard, R. Widmer, Y. deHazan, T. Graule, J. Michler, L. Philippe, Electrodeposition of gold thin films with controlled morphologies and their applications in electrocatalysis and SERS, *Nanotechnology*. 23 (2012) 255705. doi:10.1088/0957-4484/23/25/255705.
- [2] R. Alvarez, J.M. García-Martín, M. Macías-Montero, L. Gonzalez-Garcia, J.C. González, V. Rico, J. Perlich, J. Cotrino, A.R. González-Elipe, A. Palmero, Growth regimes of porous gold thin films deposited by magnetron sputtering at oblique incidence: from compact to columnar microstructures, *Nanotechnology*. 24 (2013) 045604. doi:10.1088/0957-4484/24/4/045604.
- [3] J. Siegel, O. Lyutakov, V. Rybka, Z. Kolská, V. Švorčík, Properties of gold nanostructures sputtered on glass, *Nanoscale Res. Lett.* 6 (2011) 96. doi:10.1186/1556-276X-6-96.
- [4] P. Lansåker, Gold-based nanoparticles and thin films: applications to green nanotechnology, *Acta Universitatis Upsaliensis*, 2012.

- [5] O. Szabó, S. FlickyngeroVá, T. Ignat, I. Novotný, V. Tvarozek, Gold nanostructures sputtered on zinc oxide thin film and corning glass substrates, *Facta Univ. - Ser. Electron. Energ.* 29 (2016) 77–88. doi:10.2298/FUEE1601077S.
- [6] L. Sun, D. Zhao, M. Ding, H. Zhao, Z. Zhang, B. Li, D. Shen, A white-emitting ZnO–Au nanocomposite and its SERS applications, *Appl. Surf. Sci.* 258 (2012) 7813–7819. doi:10.1016/j.apsusc.2012.04.039.
- [7] C.F. Klingshirn, B.K. Meyer, A. Waag, A. Hoffmann, J. Geurts, *Zinc Oxide*, Springer Berlin Heidelberg, Berlin, Heidelberg, 2010. doi:10.1007/978-3-642-10577-7.
- [8] O. Szabó, S. Kováčová, V. Tvarozek, I. Novotný, P. Šutta, M. Netrvalová, D. Rossberg, P. Schaaf, Nanocolumnar growth of sputtered ZnO thin films, *Thin Solid Films.* 591 (2015) 230–236. doi:10.1016/j.tsf.2015.04.009.
- [9] R.R. LaPierre, Nanowires for next generation photovoltaics, in: N.P. Kobayashi, A.A. Talin, A.V. Davydov, M.S. Islam (Eds.), 2013: p. 88200A. doi:10.1117/12.2026241.
- [10] A. Lakhtakia, M.C. Demirel, M.W. Horn, J. Xu, Six Emerging Directions in Sculptured-Thin-Film Research, in: *Adv. Solid State Phys.*, Springer Berlin Heidelberg, Berlin, Heidelberg, 2007: pp. 295–307. doi:10.1007/978-3-540-38235-5_22.
- [11] J. Dutta, S. Anantha Ramakrishna, A. Lakhtakia, Periodically patterned columnar thin films as blazed diffraction gratings, *Appl. Phys. Lett.* 102 (2013) 161116. doi:10.1063/1.4802975.
- [12] S.P. Singh, S.K. Arya, P. Pandey, B.D. Malhotra, S. Saha, K. Sreenivas, V. Gupta, Cholesterol biosensor based on rf sputtered zinc oxide nanoporous thin film, *Appl. Phys. Lett.* 91 (2007) 063901. doi:10.1063/1.2768302.
- [13] M.J.S. Spencer, Gas sensing applications of 1D-nanostructured zinc oxide: Insights from density functional theory calculations, *Prog. Mater. Sci.* 57 (2012) 437–486. doi:10.1016/j.pmatsci.2011.06.001.
- [14] M. Jacobs, S. Muthukumar, A. Panneer Selvam, J. Engel Craven, S. Prasad, Ultra-sensitive electrical immunoassay biosensors using nanotextured zinc oxide thin films on printed circuit board platforms, *Biosens. Bioelectron.* 55 (2014) 7–13. doi:10.1016/j.bios.2013.11.022.
- [15] J.N. Anker, W.P. Hall, O. Lyandres, N.C. Shah, J. Zhao, R.P. Van Duyne, Biosensing with plasmonic nanosensors, *Nat. Mater.* 7 (2008) 442–453. doi:10.1038/nmat2162.
- [16] L. De Sio, T. Placido, R. Comparelli, M. Lucia Curri, M. Striccoli, N. Tabiryan, T.J. Bunning, Next-generation thermo-plasmonic technologies and plasmonic nanoparticles in optoelectronics, *Prog. Quantum Electron.* 41 (2015) 23–70. doi:10.1016/j.pquantelec.2015.03.001.
- [17] P.K. Sahoo, D. Wang, P. Schaaf, Retraction: Tunable plasmon resonance of semi-spherical nanoporous gold nanoparticles (2014 *Mater. Res. Express* 1 035018), *Mater. Res. Express.* 2 (2015) 039701. doi:10.1088/2053-1591/2/3/039701.
- [18] L. Guo, J.A. Jackman, H.-H. Yang, P. Chen, N.-J. Cho, D.-H. Kim, Strategies for enhancing the sensitivity of plasmonic nanosensors, *Nano Today.* 10 (2015) 213–239. doi:10.1016/j.nantod.2015.02.007.
- [19] D. Wang, R. Ji, A. Albrecht, P. Schaaf, Ordered arrays of nanoporous gold nanoparticles, *Beilstein J. Nanotechnol.* 3 (2012) 651–657. doi:10.3762/bjnano.3.74.
- [20] M. Lončarić, J. Sancho-Parramon, H. Zorc, S. Šegota, P. Dubček, S. Bernstorff, Optical and structural characterization of gold island films on glass substrates, *Thin Solid Films.* 591 (2015) 204–209. doi:10.1016/j.tsf.2015.04.031.
- [21] A. Vaskevich, I. Rubinstein, Localized Surface Plasmon Resonance (LSPR) Transducers Based on Random Evaporated Gold Island Films: Properties and Sensing Applications, in: A. Dmitriev (Ed.), *Nanoplasmonic Sens.*, Springer New York, New York, NY, 2012: pp. 333–368. doi:10.1007/978-1-4614-3933-2_14.
- [22] J. Siegel, O. Kvítek, O. Lyutakov, A. Řezníčková, V. Švorčík, Low pressure annealing of gold nanostructures, *Vacuum.* 98 (2013) 100–105. doi:10.1016/j.vacuum.2013.03.019.

- [23] X. Sun, H. Li, The influence of cyclic deposition and anneal on growth of isolated and well-dispersed Au nanoisland arrays, *Appl. Surf. Sci.* 357 (2015) 1836–1842. doi:10.1016/j.apsusc.2015.08.190.
- [24] K.A. Willets, R.P. Van Duyne, Localized Surface Plasmon Resonance Spectroscopy and Sensing, *Annu. Rev. Phys. Chem.* 58 (2007) 267–297. doi:10.1146/annurev.physchem.58.032806.104607.
- [25] P.K. Jain, W. Huang, M.A. El-Sayed, On the Universal Scaling Behavior of the Distance Decay of Plasmon Coupling in Metal Nanoparticle Pairs: A Plasmon Ruler Equation, *Nano Lett.* 7 (2007) 2080–2088. doi:10.1021/nl071008a.
- [26] V. Tvarožek, O. Szabó, I. Novotný, S. Kováčová, J. Škriniarová, P. Šutta, Plasmonic behaviour of sputtered Au nanoisland arrays, *Appl. Surf. Sci.* 395 (2017) 241–247. doi:10.1016/j.apsusc.2016.04.183.
- [27] I. Novotny, S. Flickyngero, V. Tvarozek, P. Sutta, M. Netrvalova, D. Rossberg, P. Schaaf, Surface morphology and crystalline structure of sequentially sputtered ZnO nanocoatings, *Appl. Surf. Sci.* 312 (2014) 167–171. doi:10.1016/j.apsusc.2014.05.121.
- [28] I. Novotny, V. Tvarozek, P. Sutta, M. Netrvalova, J. Novak, I. Vavra, P. Elias, Preparation of shell nanocrystalline Ga-doped ZnO ultra-thin films by sputtering, in: *IEEE*, 2012: pp. 269–271. doi:10.1109/MIEL.2012.6222851.
- [29] C. Ratsch, J.A. Venables, Nucleation theory and the early stages of thin film growth, *J. Vac. Sci. Technol. Vac. Surf. Films.* 21 (2003) S96–S109. doi:10.1116/1.1600454.
- [30] A. Mazor, D.J. Srolovitz, P.S. Hagan, and B.G. Bukiet, Columnar growth in thin films, *Phys. Rev. Lett.* 60 (1988) 424–427. doi:10.1103/PhysRevLett.60.424.
- [31] V. Tvarozek, I. Novotny, P. Sutta, S. Flickyngero, K. Schtere, E. Vavrinsky, Influence of sputtering parameters on crystalline structure of ZnO thin films, *Thin Solid Films.* 515 (2007) 8756–8760. doi:10.1016/j.tsf.2007.03.125.
- [32] Y.D. Fan, X.P. Li, J. Yang, J.P. Li, Microscopic Model for Columnar Growth of Thin Films, *Phys. Status Solidi A.* 134 (1992) 157–166. doi:10.1002/pssa.2211340114.
- [33] L. Eckertová, *Physics of thin films*, 2nd rev. ed, Plenum Press, New York, 1986.
- [34] J.G. Lu, Z.Z. Ye, Y.J. Zeng, L.P. Zhu, L. Wang, J. Yuan, B.H. Zhao, Q.L. Liang, Structural, optical, and electrical properties of (Zn,Al)O films over a wide range of compositions, *J. Appl. Phys.* 100 (2006) 073714. doi:10.1063/1.2357638.
- [35] H. Morkoç, Ü. Özgür, *Zinc oxide: fundamentals, materials and device technology*, Wiley-VCH, Weinheim, 2009.
- [36] A.C. Gâlcă, M. Secu, A. Vlad, J.D. Pedarnig, Optical properties of zinc oxide thin films doped with aluminum and lithium, *Thin Solid Films.* 518 (2010) 4603–4606. doi:10.1016/j.tsf.2009.12.041.
- [37] N. Baydogan, T. Ozdurmusoglu, H. Cimenoglu, A.B. Tugrul, Refractive Index and Extinction Coefficient of ZnO:Al Thin Films Derived by Sol-Gel Dip Coating Technique, *Defect Diffus. Forum.* 334–335 (2013) 290–293. doi:10.4028/www.scientific.net/DDF.334-335.290.
- [38] J. Novák, P. Šutta, I. Vávra, P. Eliáš, S. Hasenöhrl, A. Laurenčíková, I. Novotný, Columnar microstructure of the ZnO shell layer deposited on the GaP nanowires, *Appl. Surf. Sci.* 312 (2014) 162–166. doi:10.1016/j.apsusc.2014.05.198.
- [39] X. You, J.H. Pikul, W.P. King, J.J. Pak, Zinc oxide inverse opal enzymatic biosensor, *Appl. Phys. Lett.* 102 (2013) 253103. doi:10.1063/1.4811411.
- [40] E. Topoglidis, A.E. Cass, B. O'Regan, J.R. Durrant, Immobilisation and bioelectrochemistry of proteins on nanoporous TiO₂ and ZnO films, *J. Electroanal. Chem.* 517 (2001) 20–27. doi:10.1016/S0022-0728(01)00673-8.
- [41] J. Zhou, N.S. Xu, Z.L. Wang, Dissolving Behavior and Stability of ZnO Wires in Biofluids: A Study on Biodegradability and Biocompatibility of ZnO Nanostructures, *Adv. Mater.* 18 (2006) 2432–2435. doi:10.1002/adma.200600200.

- [42] H.-J. Park, S. Mho, Electrochemical Impedance Spectroscopy and Voltammetry of Zinc in Dilute Alkaline Solutions., *Anal. Sci.* 13 (1997) 311–316. doi:10.2116/analsci.13.Supplement_311.
- [43] R. Renuka, L. Srinivasan, S. Ramamurthy, A. Veluchamy, N. Venkatakrishnan, Cyclic voltammetric study of zinc and zinc oxide electrodes in 5.3 M KOH, *J. Appl. Electrochem.* 31 (2001) 655–661.
- [44] J. Wang, *Analytical electrochemistry*, 3rd ed, Wiley-VCH, Hoboken, N.J, 2006.
- [45] C.A. Schneider, W.S. Rasband, K.W. Eliceiri, NIH Image to ImageJ: 25 years of image analysis, *Nat. Methods.* 9 (2012) 671–675. doi:10.1038/nmeth.2089.
- [46] T. Ignat, M.-A. Husanu, R. Munoz, M. Kusko, M. Danila, C.M. Teodorescu, Gold nano-island arrays on silicon as SERS active substrate for organic molecule detection, *Thin Solid Films.* 550 (2014) 354–360. doi:10.1016/j.tsf.2013.10.151.
- [47] P.K. Jain, M.A. El-Sayed, Surface Plasmon Coupling and Its Universal Size Scaling in Metal Nanostructures of Complex Geometry: Elongated Particle Pairs and Nanosphere Trimers, *J. Phys. Chem. C.* 112 (2008) 4954–4960. doi:10.1021/jp7120356.
- [48] M.A. Otte, B. Sepulveda, Figures of Merit for Refractometric LSPR Biosensing, in: A. Dmitriev (Ed.), *Nanoplasmonic Sens.*, Springer New York, New York, NY, 2012: pp. 317–331. doi:10.1007/978-1-4614-3933-2_13.
- [49] S.A. Maier, *Plasmonics: Fundamentals and Applications*, Springer US, New York, NY, 2007. doi:10.1007/0-387-37825-1.
- [50] J. Hammond, N. Bhalla, S. Rafiee, P. Estrela, Localized Surface Plasmon Resonance as a Biosensing Platform for Developing Countries, *Biosensors.* 4 (2014) 172–188. doi:10.3390/bios4020172.
- [51] Y. Cao, D. Li, F. Jiang, Y. Yang, Z. Huang, Engineering Metal Nanostructure for SERS Application, *J. Nanomater.* 2013 (2013) 1–12. doi:10.1155/2013/123812.
- [52] ADEPT, Proceedings of ADEPT, 3rd International Conference on Advances in Electronic and Photonic Technologies, Štrbské Pleso, High Tatras, Slovakia, June 1-4, 2015, University of Žilina, Žilina, 2015.
- [53] G. Barbillon, J.-L. Bijeon, J. Plain, M.L. de la Chapelle, P.-M. Adam, P. Royer, Biological and chemical gold nanosensors based on localized surface plasmon resonance, *Gold Bull.* 40 (2007) 240–244. doi:10.1007/BF03215587.
- [54] S.S. Aćimović, M.P. Kreuzer, R. Quidant, Engineering Through Mode Shaping and Lithographical Nanofabrication of Ultrasensitive Nano-plasmonic Sensors for Molecular Detection, in: A. Dmitriev (Ed.), *Nanoplasmonic Sens.*, Springer New York, New York, NY, 2012: pp. 267–287. doi:10.1007/978-1-4614-3933-2_11.
- [55] O. Szabo, V. Tvarozek, S. Kovacova, I. Novotny, Gold nanoisland arrays prepared by sputtering and bio-functionalization of their surfaces, in: 2016 11th Int. Conf. Adv. Semicond. Devices Microsyst. ASDAM, IEEE, Smolenice, Slovakia, 2016: pp. 125–128. doi:10.1109/ASDAM.2016.7805911.
- [56] E. Barsoukov, J.R. Macdonald, eds., *Impedance Spectroscopy: Theory, Experiment, and Applications*, John Wiley & Sons, Inc., Hoboken, NJ, USA, 2005. doi:10.1002/0471716243.

LIST OF PUBLICATIONS

Ing. Ondrej Szabó

ADC Scientific/scholarly papers published in the journals registered in the Current Contents Connect database and published abroad

- ADC01 **SZABÓ, Ondrej** - KOVÁČOVÁ, Soňa - TVAROŽEK, Vladimír - NOVOTNÝ, Ivan - ŠUTTA, Pavol - NETRVALOVÁ, Marie - ROSSBERG, Diana - SCHAAF, Peter. Nanocolumnar growth of sputtered ZnO thin films. In *Thin Solid Films*. Vol. 591, Part B (2015), s. 230-236. ISSN 0040-6090. V databáze: CC: 000362008000015.
- ADC02 TVAROŽEK, Vladimír - **SZABÓ, Ondrej** - NOVOTNÝ, Ivan - KOVÁČOVÁ, Soňa - ŠKRINIAROVÁ, Jaroslava - ŠUTTA, Pavol. Plasmonic behaviour of sputtered Au nanoisland arrays. In *Applied Surface Science*. Vol. 395, (2017), s. 241-247. ISSN 0169-4332. V databáze: CC: 000390428300041.

ADF Scientific/scholarly papers published in the journals not registered in the Current Contents Connect database and published in the country of residence

- ADF01 **SZABÓ, Ondrej** - PERNÝ, Milan - ŠÁLY, Vladimír - PACKA, Juraj - FLICKYNGEROVÁ, Soňa - VAVRINSKÝ, Erik. Automatizované pracovisko na meranie parametrov a parazitných odporov slnečných článkov. In *EE časopis pre elektrotechniku, elektroenergetiku, informačné a komunikačné technológie*. Roč. 19, č. 3 (2013), s.12-15. ISSN 1335-2547.

ADM Scientific/scholarly papers published in the journals registered in the databases Web of Science and SCOPUS and published abroad

- ADM01 **SZABÓ, Ondrej** - FLICKYNGEROVÁ, Soňa - IGNAT, Teodora - NOVOTNÝ, Ivan - TVAROŽEK, Vladimír. Gold nanostructures sputtered on zinc oxide thin film and corning glass substrates. In *Facta Universitatis*. Vol. 29, No. 1 (2016), s. 77-88. ISSN 0353-3670. V databáze: WOS: 000382945500006.

AFC Published conference papers presented at conferences abroad

- AFC01 SHTEREVA, Krasmira - TVAROŽEK, Vladimír - KOVÁČ, Jaroslav jr. - NOVOTNÝ, Ivan - **SZABÓ, Ondrej** - VOJS, Marian - KOVÁČOVÁ, Soňa. Electrical and optical characterization of sputtered ZnO:Ga thin films doped with nitrogen. In *ISSE 2017 : 40th international spring seminar on electronics technology. Sofia, Bulgaria. May 10-14, 2017*. Piscataway : IEEE, 2017, [5] s. ISSN 2161-2536. ISBN 978-1-5386-0583-7. V databáze: IEEE ; WOS: 000426973000002.

- AFC02 **SZABÓ, Ondrej** - PERNÝ, Milan - LELÁK, Jaroslav - ŠÁLY, Vladimír - VÁRY, Michal - FLICKYNGEROVÁ, Soňa - VAVRINSKÝ, Erik. DC Diagnostics of Solar Cell Parameters. In *Diagnostika '13 : International Conference on Diagnostics in Electrical Engineering CDEE 2013. Pilsen, Czech Republic, September 2-4, 2013.* Pilsen : University of West Bohemia, 2013, s.215-218. ISBN 978-80-261-0210-6.
- AFC03 **SZABÓ, Ondrej** - FLICKYNGEROVÁ, Soňa - TVAROŽEK, Vladimír - NOVOTNÝ, Ivan. Sputtered gold nanostructures. In *29th International conference on microelectronics : proceedings; MIEL 2014, Belgrade, Serbia; 12-15 May 2014.* Danvers : IEEE Electron Devices Society, 2014, s. 245-247. ISBN 978-1-4799-5295-3.
- AFD Published conference papers presented at conferences in the country of residence**
- AFD01 FLICKYNGEROVÁ, Soňa - IGNAT, Teodora - KOVÁČ, Jaroslav Jr. - **SZABÓ, Ondrej** - NOVOTNÝ, Ivan - TVAROŽEK, Vladimír - LABUDA, Ján. SERS properties of RF sputtering gold nanoparticles on ZnO:Al. In *ADEPT 2014 : 2nd International Conference on Advances in Electronic and Photonic Technologies; Tatranská Lomnica, Slovakia; June 1-4, 2014.* 1.vyd. Žilina : University of Žilina, 2014, s. 176-179. ISBN 978-80-554-0881-1.
- AFD02 MICHNIAK, Pavol - VOJS, Marian - MARTON, Marián - **SZABÓ, Ondrej** - BEHÚL, Miroslav - VESELÝ, Marián - REDHAMMER, Robert - GRIESELER, Rolf - SCHAAF, Peter. Boron doped diamond thin films - structural and electrical properties. In *ADEPT 2014 : 2nd International Conference on Advances in Electronic and Photonic Technologies; Tatranská Lomnica, Slovakia; June 1-4, 2014.* 1.vyd. Žilina : University of Žilina, 2014, s. 192-195. ISBN 978-80-554-0881-1.
- AFD03 POPOVIČ, Marián - VAVRINSKÝ, Erik - **SZABÓ, Ondrej** - TVAROŽEK, Vladimír. Development of multifunctional device for measuring of the bioelectrical impedance. In *ELITECH'15 [elektronický zdroj] : 17th Conference of doctoral students. Bratislava, Slovak Republic, May 25, 2015.* 1. vyd. Bratislava : Nakladateľstvo STU, 2015, CD-ROM, [5] s. ISBN 978-80-227-4358-7.
- AFD04 **SZABÓ, Ondrej** - PERNÝ, Milan - FLICKYNGEROVÁ, Soňa - VAVRINSKÝ, Erik - KOVÁČ, Jaroslav Jr. - TVAROŽEK, Vladimír - ŠÁLY, Vladimír. Automated Workplace for Measurement of PV Cells. In *ADEPT 2013 : 1st International Conference on Advances in Electronic and Photonic Technologies. Nový Smokovec, High Tatras, Slovakia, June 2-5, 2013.* 1. vyd. Žilina : University of Žilina, 2013, s.109-112. ISBN 978-80-554-0689-3.
- AFD05 **SZABÓ, Ondrej** - FLICKYNGEROVÁ, Soňa - TVAROŽEK, Vladimír. The SEM Image Evaluation of Sputtered Nanostructured Au Films. In *VESELÝ, Marián.16. Škola vákuovej techniky. Perspektívne vákuové metódy a technológie : zborník, Štrbské Pleso, Slovak Republic, 10 -13 október 2013.* 1. vyd. Bratislava : Slovenská vákuová spoločnosť, 2013, s.105-108. ISBN 978-80-971179-2-4.

- AFD06 **SZABÓ, Ondrej** - FLICKYNGEROVÁ, Soňa - TVAROŽEK, Vladimír - NOVOTNÝ, Ivan. Surface morphology and optical properties of Au nanoparticles on ZnO:Al thin films. In *ADEPT 2014 : 2nd International Conference on Advances in Electronic and Photonic Technologies; Tatranská Lomnica, Slovakia; June 1-4, 2014*. 1.vyd. Žilina : University of Žilina, 2014, s. 180-183. ISBN 978-80-554-0881-1.
- AFD07 **SZABÓ, Ondrej** - KOVÁČOVÁ, Soňa - ŠKRINIAROVÁ, Jaroslava - ROSSBERG, Diana - TVAROŽEK, Vladimír. Effect of annealing on properties sputtered Au nanostructures. In *ADEPT 2015 : 3rd international conference on advances in electronic and photonic technologies. Štrbské Pleso, High Tatras, Slovakia. June 1-4, 2015*. 1. vyd. Žilina : University of Žilina, 2015, S. 120-123. ISBN 978-80-554-1033-3.
- AFD08 **SZABÓ, Ondrej** - NOVOTNÝ, Ivan - KOVÁČOVÁ, Soňa - TVAROŽEK, Vladimír. Sputtering of gold nanoisland arrays through the gradient of film thicknesses. In *ADEPT 2016 : 4th International conference on advances in electronic and photonic technologies. Tatranská Lomnica, Slovakia. June 20-23, 2016*. 1. vyd. Žilina : University of Žilina, 2016, S. 79-82. ISBN 978-80-554-1226-9.
- AFD09 **SZABÓ, Ondrej** - TVAROŽEK, Vladimír - KOVÁČOVÁ, Soňa - NOVOTNÝ, Ivan. Gold nanoisland arrays prepared by sputtering and bio-functionalization of their surfaces. In *ASDAM 2016 : 11th International conference on advanced semiconductor devices and microsystems. Smolenice, Slovakia. November 13-16, 2016*. Danvers : IEEE, 2016, S. 125-128. ISBN 978-1-5090-3081-1. V databáze: IEEE ; WOS: 000392530900031 ; SCOPUS: 2-s2.0-85011024547.
- AFD10 **SZABÓ, Ondrej** - TVAROŽEK, Vladimír - NOVOTNÝ, Ivan - ŠUTTA, Pavol - MIKOLÁŠEK, Miroslav - KOVÁČOVÁ, Soňa - SCHAAF, Peter. Influence of titanium ultrathin non-continuous film on sputtered gold nanoisland arrays. In *ADEPT 2017 : 5th International conference on advances in electronic and photonic technologies. Podbanské, Slovakia. June 19-22, 2017*. 1. vyd. Žilina : University of Žilina, 2017, S. 279-282. ISBN 978-80-554-1342-6.
- AFD11 ŠKRINIAROVÁ, Jaroslava - **SZABÓ, Ondrej** - NOVOTNÝ, Ivan - TVAROŽEK, Vladimír. Evaluation of sputtered nanoisland arrays by AFM and SEM. In *ADEPT 2016 : 4th International conference on advances in electronic and photonic technologies. Tatranská Lomnica, Slovakia. June 20-23, 2016*. 1. vyd. Žilina : University of Žilina, 2016, S. 155-158. ISBN 978-80-554-1226-9.
- AFG Published abstracts of conference papers presented at conferences abroad**
- AFG01 FLICKYNGEROVÁ, Soňa - TVAROŽEK, Vladimír - **SZABÓ, Ondrej** - NOVOTNÝ, Ivan - ŠUTTA, Pavol. Nanocolumnar growth of sputtered ZnO thin films. In *16th International Conference on Thin Films : Programme and book of abstracts. Dubrovnik, Croatia; 13-16 October 2014*. Zagreb : Croatian Vacuum Society, 2014, S. 126. ISBN 978-953-98154-4-6.

AFG02 **SZABÓ, Ondrej** - NOVOTNÝ, Ivan - TVAROŽEK, Vladimír - ŠUTTA, Pavol - NETRVALOVÁ, Marie - KOVÁČOVÁ, Soňa. The formation of Au plasmonic nanostructures on ZnO thin films by the sputtering. In *SURFINT - SREN IV : Progress in applied surface, interface and thin film science. Florence, Italy. 23-26. November 2015*. Bratislava : Comenius University, 2015, S. 138-139. ISBN 978-80-223-3975-9.

AFG03 TVAROŽEK, Vladimír - **SZABÓ, Ondrej** - NOVOTNÝ, Ivan - ŠKRINIAROVÁ, Jaroslava - ŠUTTA, Pavol - NETRVALOVÁ, Marie - IGNAT, Teodora - KOVÁČOVÁ, Soňa. Plasmonic behaviour of sputtered Au nanostructures on glass substrate. In *SURFINT - SREN IV : Progress in applied surface, interface and thin film science. Florence, Italy. 23-26. November 2015*. Bratislava : Comenius University, 2015, S. 158-159. ISBN 978-80-223-3975-9.

AFH Published abstracts of conference papers presented at conferences in the country of residence

AFH01 FLICKYNGEROVÁ, Soňa - **SZABÓ, Ondrej** - NOVOTNÝ, Ivan - TVAROŽEK, Vladimír - ŠUTTA, Pavol - NETRVALOVÁ, Marie. Nanostructured Ultra-Thin Films of Gold Prepared by Sputtering. In *8th Solid State Surfaces and Interfaces : Extended Abstract Book. Smolenice Castle, Slovak Republic, November 25-28, 2013*. Bratislava : Comenius University, 2013, s.45. ISBN 978-80-223-3501-0.

AFH02 POPOVIČ, Marián - VAVRINSKÝ, Erik - **SZABÓ, Ondrej**. Vývoj viacúčelového zariadenia na meranie bioelektrickej impedancie. In *Lekárska fyzika a biofyzika na začiatku 21. storočia 2 : Aplikácia fyziky v medicíne : 2. vedecko-odborná konferencia s medzinárodnou účasťou. Bratislava, Slovenská republika. 10. september 2015*. Bratislava : Univerzita Komenského v Bratislave, 2015, S. 39. ISBN 978-80-223-3953-7.

BDF Specialised papers published in the journals not registered in the Current Contents Connect database and published in the country of residence

BDF01 PERNÝ, Milan - ŠÁLY, Vladimír - FLICKYNGEROVÁ, Soňa - STUHLÍKOVÁ, Ľubica - **SZABÓ, Ondrej**. Fotovoltika a jej propagácia smerom ku mladým ľuďom. In *ChemZi. Roč. 8, č. 2 (2012)*, s.108-109. ISSN 1336-7242.

BEF Specialised papers in non-reviewed (conference and non-conference) collections of papers published in the country of residence

BEF01 **SZABÓ, Ondrej** - PERNÝ, Milan - FLICKYNGEROVÁ, Soňa - VAVRINSKÝ, Erik. Vývoj meracieho pracoviska na meranie jednosmerných parametrov fotovoltických solárnych článkov. In *ŠVOČ 2013 [elektronický zdroj] : Zborník vybraných prác, Bratislava, 23. apríl 2013*. 1. vyd. Bratislava : FEI STU, 2013, s.CD ROM, s. 131-136. ISBN 978-80-227-3909-2.

BFA Published abstracts of specialised papers presented at academic events (conferences, etc.) abroad

BFA01 ŠKRINIAROVÁ, Jaroslava - KADLEČÍKOVÁ, Magdaléna - SZABÓ, Ondrej - NOVOTNÝ, Ivan - TVAROŽEK, Vladimír. Study of topology ultrathin discontinuous gold layers. In *Mikroskopie 2015*. Praha : CSMS, 2015, S. 46-47.

Statistics: Category of publishing activity

ADC	Scientific/scholarly papers published in the journals registered in the Current Contents Connect database and published abroad	2
ADF	Scientific/scholarly papers published in the journals not registered in the Current Contents Connect database and published in the country of residence	1
ADM	Scientific/scholarly papers published in the journals registered in the databases Web of Science and SCOPUS and published abroad	1
AFC	Published conference papers presented at conferences abroad	3
AFD	Published conference papers presented at conferences in the country of residence	11
AFG	Published abstracts of conference papers presented at conferences abroad	3
AFH	Published abstracts of conference papers presented at conferences in the country of residence	2
BDF	Specialised papers published in the journals not registered in the Current Contents Connect database and published in the country of residence	1
BEF	Specialised papers in non-reviewed (conference and non-conference) collections of papers published in the country of residence	1
BFA	Published abstracts of specialised papers presented at academic events (conferences, etc.) abroad	1
Total:		26